

# On the origin and properties of Ultrafaint Milky Way Satellites in a $\Lambda$ CDM Universe

Andrea V. Macciò<sup>1\*</sup>, Xi Kang<sup>1</sup>, Fabio Fontanot<sup>1</sup>, Rachel S. Somerville<sup>1,2</sup>  
Sergey Koposov<sup>1,3,4</sup>, Pierluigi Monaco<sup>5,6</sup>

<sup>1</sup> *Max-Planck-Institut für Astronomie, Königstuhl 17, 69117 Heidelberg, Germany*

<sup>2</sup> *Space Telescope Science Institute, 3700 San Martin Drive, Baltimore, MD 21218, USA*

<sup>3</sup> *Institute of Astronomy, University of Cambridge, Madingley Road, Cambridge, UK*

<sup>4</sup> *Sternberg Astronomical Institute, Universitetskii pr. 13, 119992 Moscow, Russia*

<sup>5</sup> *Dipartimento di Astronomia, Università di Trieste, via Tiepolo 11, 34131 Trieste, Italy*

<sup>6</sup> *INAF-Osservatorio Astronomico, Via Tiepolo 11, I-34131 Trieste, Italy*

submitted to MNRAS

## ABSTRACT

We study the origin and properties of satellite galaxies within Milky Way sized haloes as predicted in Cold Dark Matter based models of galaxy formation, making use of dissipationless and hydrodynamic numerical N-body techniques as well as three different semi-analytic model (SAMs) galaxy formation codes. We extract merger trees from very high-resolution dissipationless N-body simulations of four Galaxy-sized DM haloes, and use these as common input for the semi-analytic models. We present a detailed comparison of our predictions with the observational data recently obtained on the Milky Way satellite luminosity function (LF). We find that semi-analytic models with rather standard astrophysical ingredients are able to reproduce the observed luminosity function over six orders of magnitude in luminosity, down to magnitudes as faint as  $M_V = -2$ . We also perform a comparison with the actual observed number of satellites as a function of luminosity, by applying the selection criteria of the SDS survey to our simulations instead of correcting the observations for incompleteness. Using this approach we again find good agreement for both the luminosity and radial distributions of MW satellites. We investigate which physical processes in our models are responsible for shaping the predicted satellite LF, and find that tidal destruction, suppression of gas infall by a photo-ionizing background, and supernova feedback all make important contributions. For three of our dark matter haloes we have also run hydrodynamic simulations (at a lower numerical resolution) in which we also include gas cooling, star formation and stellar feedback. We find that the predictions of the numerical hydrodynamic simulations are in good agreement with those of the SAMs for the stellar mass function of satellites as well as for their radial distribution. We conclude that the number and luminosity of Milky Way satellites can be naturally accounted for within the ( $\Lambda$ )Cold Dark Matter paradigm, and this should no longer be considered a problem.

**Key words:** galaxies: haloes – cosmology:theory, dark matter, gravitation – methods: numerical, N-body simulation

## 1 INTRODUCTION

The Milky Way environment provides an excellent laboratory for astrophysics. It has been used extensively in the past decades to test theoretical models of galaxy formation.

In particular, the number density of satellites around our Galaxy has long been considered one of the major problems for the otherwise quite successful  $\Lambda$ CDM paradigm.

About a decade ago, N-body simulations attained sufficient dynamic range to reveal that in CDM models, all haloes should contain a large number of embedded sub-haloes that survive the collapse and virialization of the par-

\* maccio@mpia.de

ent structure (Klypin et al. 1999; Moore et al. 1999 and more recently Diemand et al. 2007). Although the predicted number of substructures was in reasonable agreement with observed luminosity functions in cluster sized haloes, in Milky Way sized haloes the number of predicted sub-haloes exceeded the number of observed satellites by at least an order of magnitude: the known satellite population at the time consisted of about 40 satellites with  $V_c \gtrsim 20\text{km/s}$  in the Local Group (e.g. Mateo 1998), while the simulations predicted about 300 sub-haloes with  $V_c \gtrsim 20\text{km/s}$  (Klypin et al. 1999; Moore et al. 1999).

Several astrophysical solutions to this problem have been proposed. Many authors have pointed out that accretion of gas into low-mass haloes and subsequent star formation is inefficient in the presence of a strong photoionizing background, as this background radiation raises the entropy of the gas, preventing it from accreting onto small dark matter haloes and lengthening the cooling time of that gas which has accreted (e.g. Babul & Rees 1992; Efsthathiou 1992; Thoul & Weinberg 1996; Quinn, Katz, & Efsthathiou 1996). Several studies showed quantitatively that this suppression of gas infall by cosmic reionization could plausibly reconcile the observed and predicted numbers of “classical” ( $M_V \lesssim -10$ ) Local Group satellites (Bullock et al. 2000, Somerville 2002, Ricotti, Gnedin & Shull 2002, Benson et al. 2002, Read et al. 2006). It was also pointed out that tidal stripping and heating as satellites orbited in the potential of the larger galaxy could cause dramatic mass loss, even decreasing the circular velocity in the inner parts of the sub-halo (Kravtsov, Gnedin & Klypin 2004; Taylor & Babul 2004; Zentner et al. 2005). Thus many Local Group satellites may inhabit dark matter (sub-)haloes that are much less massive than they were at the time that they were accreted by their host halo.

In recent years the Sloan Digital Sky Survey (SDSS: Adelman-McCarthy et al. 2008) has changed our view of the Milky Way and its environment. The SDSS has made it possible to carry out a systematic survey for satellite galaxies, which are detectable through their resolved stellar populations down to extremely low surface brightness. As a result the number of known dwarf spheroidals has doubled in the recent past (e.g. Willman et al. 2005, Zucker et al. 2006; Belokurov et al. 2007; Irwin et al. 2007, Gilmore et al. 2007). Spectroscopic surveys subsequently measured the velocity dispersions of these systems, and confirmed their galactic nature (Martin et al. 2007, Simon & Geha 2007). This recently discovered population of ultra faint satellites has posed new challenges for models of galaxy formation and opened the possibility to test the  $\Lambda\text{CDM}$  paradigm at very small mass scales (e.g. Strigari et al. 2008, Macciò et al. 2009).

These new observations have made it possible to probe the faint end of the luminosity function of Milky Way satellites, down to luminosities as faint as  $100 L_\odot$ . Moreover the homogeneous sky coverage of the SDSS enables a robust determination of the detection limits for faint satellites. Koposov et al. (2008) provided the first determination of the volume corrected Milky Way satellite luminosity function down to these ultra-faint limits, by assuming various simple radial distribution functions for the satellite population and applying the SDSS detection limits.

In light of the discovery of the new ultra-faint dwarf population and the improvements in the numerical mod-

elling of galaxy formation, it is now timely to revisit the issue of whether the basic properties of satellite galaxies around the Milky Way, such as their number density, radial distribution, and mass-to-light ratios, can be reproduced within current cosmological  $\Lambda\text{CDM}$ -based models. It is also interesting to ask what physical processes might plausibly give rise to this population of extremely low-luminosity galaxies.

In this paper we combine merger trees extracted from very high resolution N-body simulations with three different semi-analytic model (SAM) codes. These merger trees describe the hierarchical assembly of a Milky Way-like halo, while the SAMs are used to predict the relationship between the dark matter (sub)haloes and observable galaxy properties, allowing us to make a direct and detailed comparison with observational data. We also present predictions from re-simulations of the same dark matter haloes, including a numerical treatment of hydrodynamical processes. Due to numerical limitations these simulations are run at a lower resolution.

The goal of this work is not only to test whether the observed properties of Milky Way satellites, including the recently discovered ultra-faint population, can be reproduced within the  $\Lambda\text{CDM}$  model, but also to understand how and when this extreme population formed. We aim to understand how various mechanisms (such as SN feedback, cosmic photo-ionization, and tidal stripping) may shape the stellar content and luminosities of galaxies populating low mass dark matter substructures orbiting around Milky Way-like galaxies.

The remainder of this paper is organized as follows. In Section 2 we describe the numerical simulations. In Section 3 we briefly summarize the SAMs used in our study, highlighting the differences among the models. Section 4 contains a detailed description of the observational data used in this work. In Section 5 we compare the luminosity function, stellar mass function and radial distribution of simulated satellites with observational data. Finally in Section 6 we present our main conclusions.

## 2 SIMULATIONS

We perform dissipationless and hydrodynamical N-body simulations for this study. The N-body simulations were obtained using PKDGRAV, a treecode written by Joachim Stadel and Thomas Quinn (Stadel 2001). The initial conditions are generated with the GRAFIC2 package (Bertschinger 2001). The starting redshift  $z_i$  is set to the time when the standard deviation of the smallest density fluctuations resolved within the simulation box reaches 0.2 (the smallest scale resolved within the initial conditions is defined as twice the intra-particle distance). The cosmological parameters are chosen to be:  $\Omega_\Lambda=0.732$ ,  $\Omega_m=0.268$ ,  $\Omega_b=0.044$ ,  $h = 0.71$  and  $\sigma_8 = 0.9$ , and are in reasonable agreement with the recent WMAP mission results (Komatsu et al. 2009).

We selected four candidate haloes with a mass similar to the mass of our Galaxy ( $M \sim 10^{12} M_\odot$ ) from an existing low resolution dark matter simulation ( $300^3$  particles within 90 Mpc) and re-simulated them at higher resolution. Our high resolution haloes all have a quiet merging history with no major merger after  $z = 2$ , and thus are likely to host a disk galaxy at the present time (with the excep-

**Table 1.** Dark Matter Halo parameters

| Halo             | Mass<br>( $10^{12}h^{-1}M_{\odot}$ ) | $N_{\text{part}}$<br>( $10^6$ ) | $R_{\text{vir}}$<br>(kpc/h) | $V_{\text{circ}}$<br>(km/s) | Hydro |
|------------------|--------------------------------------|---------------------------------|-----------------------------|-----------------------------|-------|
| G0               | 0.88                                 | 2.12                            | 197                         | 178                         | yes   |
| G1               | 1.22                                 | 2.93                            | 219                         | 188                         | yes   |
| G2               | 1.30                                 | 3.12                            | 250                         | 203                         | yes   |
| G3               | 2.63                                 | 5.64                            | 268                         | 236                         | no    |
| G1 <sub>HR</sub> | 1.15                                 | 31.5                            | 211                         | 184                         | no    |

tion of G3, which we discuss further below). The standard high resolution runs are  $12^3$  times more resolved in mass than the initial simulation: the dark matter particle mass is  $m_d = 4.16 \times 10^5 h^{-1} M_{\odot}$ , where each dark matter particle has a spline gravitational softening of  $355 h^{-1}$  pc. For each simulation we stored more than 50 outputs from redshift 20 to redshift zero, in order to construct detailed merger trees. Some of the main properties of the re-simulated haloes are listed in Table 1. One of the haloes, namely G3, has a mass greater than the expected mass of the MW and has experienced a major merger at  $z=1.5$  so it is likely to host an elliptical galaxy. In order to check possible resolution effects (especially in the construction of the merger tree) we re-simulated one of the haloes (namely G1) with higher resolution ( $27^3$  times with respect to the low resolution), with more than 32 million particles within the virial radius (G1<sub>HR</sub> in Table 1), reaching a dark matter particle mass of  $m = 3.65 \times 10^4 h^{-1} M_{\odot}$ .

The hydrodynamical simulations were performed with GASOLINE, a multi-stepping, parallel TreeSPH  $N$ -body code (Wadsley et al. 2004). We include radiative and Compton cooling for a primordial mixture of hydrogen and helium. The star formation algorithm is based on a Jeans instability criteria (Katz 1992), where gas particles in dense, unstable regions and in convergent flows spawn star particles at a rate proportional to the local dynamical time (see Governato et al. 2004). The star formation efficiency was set to 0.1, but in the adopted scheme its precise value has only a minor effect on the star formation rate (Katz 1992). The code also includes supernova feedback as described by Stinton et al. (2006), and a cosmic UV background following Haardt & Madau (1996); see Governato et al. (2007) for a more detailed description of the code.

Due to computational limitations we were forced to reduce the numerical resolution in these dissipational runs. We increased the initial resolution by a factor of  $8^3$  and we included a gaseous component within the entire high resolution region. The masses of the dark matter and gaseous particles are respectively  $m_d = 1.17 \times 10^6 h^{-1} M_{\odot}$  and  $m_g = 2.3 \times 10^5 h^{-1} M_{\odot}$ . The dark matter has a spline gravitational softening length of  $500 h^{-1}$  pc and there are about  $10^6$  particles for each component (dark and gas) in the high resolution region. These hydro simulations will be described in more detail (with particular attention to the properties of the central galaxy) in a forthcoming paper (Hernandez et al. in prep).

## 2.1 Finding Haloes and Subhaloes

For the purpose of constructing accurate merger trees for each simulated halo, we analyse 53 output times between  $z = 20$  and  $z = 0$ . For each snapshot, we look for all the virialized haloes within the high resolution region using a Spherical Overdensity (SO) algorithm. Candidate groups with a minimum of  $N_f = 50$  particles are selected using a FoF algorithm with linking length  $\phi = 0.2 \times d$  (the average particle separation). We then: (i) find the point  $C$  where the gravitational potential is a minimum; (ii) determine the radius  $\bar{r}$  of a sphere centered on  $C$ , where the density contrast is  $\Delta_{\text{vir}}$ , with respect to the critical density of the Universe. Using all particles in the corresponding sphere, we iterate the above procedure until we converge onto a stable particle set. We use a time varying virial density contrast  $\Delta_{\text{vir}}$ , whose value is determined using the fitting formula presented in Mainini et al. (2003), based on linear theory and the spherical top-hat collapse model. We include in the halo catalogue all the haloes with more than 100 particles (see Macciò et al. 2007, 2008 for further details on our halo finding procedure).

The SO algorithm is extremely fast and efficient in finding virialized structures but it is not able to find substructures within them. To find bound structures within the virial radius of our haloes at  $z = 0$  we use SKID (Stadel 2001); it calculates local densities using an SPH kernel, then particles are moved along the density gradient until they oscillate around a point (i.e. move less than some length  $l$ ). They are then linked together using the friends-of-friends algorithm with this same  $l$  as a linking length. SKID with  $l = 4\epsilon_0$  (where  $\epsilon_0$  is the force resolution of the simulation) adequately identifies the smallest subhaloes and the centers of the largest subhaloes. At redshift  $z = 0$  this value of  $l$  usually underestimates the mass of the small subhaloes that are inside the virial radius of the main halo and close to its center; using  $l = 10\epsilon_0$  can cure this, but then some of the small subhaloes are missed. We therefore use a combination of the subhalo catalogues obtained with these two linking lengths in order to obtain robust estimates of their properties.

## 2.2 Merger tree construction

We mark all the particles within 1.5 times the virial radius of a given “root” halo at  $z = 0$  and then track them back to the previous output time. We then make a list of all haloes at that earlier output time containing marked particles, recording the number of marked particles contained in each one. In addition we record the number of particles that are not in any halo in the previous output time and we consider them to be *smoothly* accreted.

We use the two criteria suggested in Wechsler et al. (2002) for halo 1 at one output time to be labeled a “progenitor” of halo 2 at the subsequent output time. In our language, halo 2 will then be labeled as a “descendant” of halo 1 if i) more than 50% of the particles in halo 1 end up in halo 2 or if ii) more than 75% of halo 1 particles that end up in any halo at time step 2 end up in halo 2 (this second criterion is mainly relevant during major mergers). Thus a halo can have only one descendant but there is no limit to the number of progenitors. On average there are 20,000 progenitors for haloes G0-G3, while the number of progenitors for the G1<sub>HR</sub> run is close to 100,000.

We find evidence for a so-called ‘backsplash’ subhalo population (e.g. Knebe et al. 2008). These haloes have orbits that bring them inside the virial radius of their host, but then take them back outside the virial radius at some later time; i.e., there is no unique “accretion” time for these (sub)-haloes. Because semi-analytic models are not set up to handle this behavior in a sensible manner, we treat these haloes in two different ways according to their final fate: i) If after having been inside the main halo, the backsplash halo survives as an isolated halo until the present time, it is removed from the progenitor list of the parent halo (i.e. it is removed from the merger tree); ii) if the halo is accreted again by the main halo and remains within it until the present time, then it is considered to have been accreted the first time it entered the main halo. In case ii), the semi-analytic model treats these sub-haloes as though they were within the virial radius of the main halo from the first accretion time onwards. Backsplash haloes account for roughly 10% of the total progenitor number but they contribute less than 1% to the final halo mass.

We have not constructed merger trees from the hydrodynamical simulations, due to their limited mass resolution. In the following we will only make use of merger trees coming from the dissipationless N-body simulations.

### 3 SEMI-ANALYTIC MODELS

We make use of three different semi-analytic model (SAM) codes in order to predict the observable properties of galaxies that inhabit the dark matter haloes and sub-haloes identified in the  $N$ -body simulations described above. These codes (see Baugh 2006 for a detailed review on the different techniques) simulate the *ab-initio* formation and evolution of galaxies in a cosmological framework, by implementing a set of physically motivated analytic “recipes” describing the main physical processes that are believed to shape the formation of galaxies. These recipes contain free parameters whose values are calibrated using a subset of observations, typically of the properties of local galaxies. SAMs are a flexible tool for exploring the effects of processes acting at very different physical scales (from the Mpc to the sub-pc) and their interplay. A disadvantage of SAMs, however, is that they necessarily require some rather arbitrary assumptions to be made. We attempt to control for this by exploring the predictions of three independently developed codes. In the following paragraphs, we will sketch the main ingredients included in the SAMs we have adopted, but we will focus on those ingredients which are of fundamental importance at the scales in which we are interested (i.e. the faint satellite population in Milky Way-like galaxies).

We will consider predictions from the most recent implementations of three different SAMs, developed independently by different groups: (i) the Kang et al. (2005) model that has been recently updated in Kang (2008, K08 hereafter); (ii) the fiducial model of Somerville et al. (2008, S08 hereafter), which builds on the original formulation presented in Somerville & Primack (1999) and Somerville et al. (2001); (iii) MORGANA, first presented in Monaco, Fontanot & Taffoni (2007).

All SAMs assume that DM haloes are the sites where galaxy formation takes place. Therefore, a proper descrip-

tion of the assembly of these DM haloes is a key requirement. This information is usually provided in the form of a DM halo merger tree, which then constitutes the backbone of the models. Different techniques may be used to obtain these merger trees: they may be extracted from  $N$ -body simulations, or generated using Monte Carlo techniques based on the extended Press-Schechter (EPS) formalism (e.g. Somerville & Kolatt 1999; Parkinson et al. 2008), or a perturbative approach like the Lagrangian code PINOCCHIO may be used (Monaco et al. 2002). In this work, we use the four merger trees extracted from  $N$ -body simulations of the G0-G3 haloes (see section 2.2) as a common input for all our SAMs. In order to increase the statistical robustness of our results, in sec. 5.2 we also consider a larger set of realizations of merger trees obtained using EPS (for K08 and S08) and PINOCCHIO (MORGANA).

Although our simulations resolve subhaloes<sup>1</sup> we do not record the fate of subhaloes in our merger trees or make use of this information in the SAMs (unlike in e.g. Kang et al. 2005). When a subhalo is accreted, its distance from the center of the parent halo is initially either set equal to the virial radius of the parent halo at that time (K08 and S08), or extracted from a suitable distribution of radial distances (MORGANA). Moreover the orbital parameters (velocity and orbit eccentricity) for each infalling satellite are randomly selected from a given distribution (a discussion on the effects of these random orbits on our final results can be found in section 5.1). The dynamical evolution (and so the survival probability) of each subhalo is then computed by estimating the time required for the subhalo to lose all of its orbital energy due to dynamical friction against the background DM potential. These “dynamical friction” times are computed using updated variants of the classical Chandrasekhar formula, which account for tidal stripping and non-circular orbits. In particular, K08 uses the results of Jiang et al. (2008), S08 use the results of Boylan-Kolchin et al. (2008) and MORGANA implements the recipe proposed by Taffoni et al. (2003).

Subhaloes may then suffer two different fates: if a critical fraction of the initial mass is lost via tidal stripping before it reaches the center of the halo, the subhalo is considered to be tidally destroyed, and the satellite galaxy contained in it is removed from the galaxy list. In the S08 model, satellites are considered to be tidally destroyed when they are stripped below a mass corresponding to the mass within  $f_{\text{dis}} \times r_s$ , where  $f_{\text{dis}}$  is a free parameter of order 0.1 – 1 and  $r_s$  is the characteristic NFW scale radius (following the procedure suggested by Zentner & Bullock 2003 and Taylor & Babul 2004). In the K08 model, subhaloes are also stripped by tidal forces, and the mass loss is described by the model of Giocoli et al. (2008). Contrary to the S08 model, in K08 subhaloes are never tidally disrupted before they merge with the central galaxy. For the work presented here, we have considered a subhalo to be tidally destroyed if it either loses more than 98% of its mass (e.g. Penarrubia et al. 2008) or if its mass falls below  $6.5 \times 10^6 M_\odot$ , which is the minimum

<sup>1</sup> From this point on, we refer to the DM haloes living within the virial radius of larger haloes as “substructure” or “subhaloes”, while we refer to the all the galaxies except the central galaxy of the larger halo as “satellites”.

mass observed for Milky Way satellites (Strigari et al. 2008). MORGANA also includes also a simple model for the effect of tidal stripping on the baryonic mass of the satellite galaxy (see sec. 5.4). If the subhalo makes it to the center of the parent halo, then the satellite galaxy is assumed to merge with the central galaxy. None of the SAMs considered here account for mergers or encounters between satellite galaxies.

Note that because the random orbits assigned to subhaloes upon accretion may differ from the actual orbital parameters in the simulation, and of course these semi-analytic recipes are not perfect, it can occur that a particular subhalo actually survives in the N-body simulation but is destroyed or merged in the SAM. In Section 5.1, we check that the statistical distributions of subhalo masses and radii predicted by the SAMs agrees with the actual distributions found in the N-body simulations. The differences between the SAM predictions and N-body results are only noticeable for the larger mass satellites, because of their small number statistics.

As each DM halo collapses and virializes, hot gas is accreted into the potential well of the halo. In the absence of any non-gravitational heating source, the baryon fraction within each halo would be equal to the universal baryon fraction. However, in the presence of a photo-ionizing background, hot gas accretion may be suppressed in haloes with mass less than a time-dependent characteristic mass related to the Jeans mass. The fraction of baryons that can collapse into haloes of a given mass can be expressed in terms of a “filtering mass” (e.g. Gnedin 2000). This filtering mass corresponds to the mass at which haloes will only be able to accrete half of the universal baryonic content. Hydrodynamic simulations including the presence of a uniform photo-ionizing background show that after cosmic reionization occurs, the value of this filtering mass increases rapidly from  $\sim 10^7 M_\odot$  to a few times  $10^{10} M_\odot$  at  $z = 0$  (Gnedin 2000; though see Okamoto et al. 2008 and Hoefl et al. 2006). In all three SAMs, the fraction of baryons that can be accreted as hot gas is parameterized as a function of halo mass and redshift, following Gnedin (2000), using the expression:

$$f_{b,acc}(z, M_{vir}) = \frac{f_b}{[1 + 0.26 M_F(z)/M_{vir}]^3}, \quad (1)$$

where  $f_b$  is the universal baryon fraction and  $M_{vir}$  is the halo virial mass. The filtering mass as a function of redshift  $M_F(z)$  depends on the reionization history of the Universe, and is parameterized using the fitting formulae provided by Kravtsov et al. (2004). Our models assume that the universe is instantaneously and uniformly reionized at a redshift  $z_r$ . As a default, we adopt  $z_r = 7.5$ , but we explore the sensitivity to the assumed value of  $z_r$  as well as to the normalization of the filtering mass in section 5.4.1.

Once gas has been accreted by a DM halo, it can cool and collapse into a rotationally supported disk, where it can eventually reach the densities required for the onset of star formation activity. The SAMs considered here make the common assumption that new cold gas is only accreted by the *central* galaxy; satellites are starved of any new gas supply once they are accreted by the parent halo. All three of our SAMs only include standard atomic cooling and do not account for the modification of the cooling rate by the photo-ionizing background (see e.g. Benson et al. 2002). Therefore, there is a sharp cutoff in the cooling below  $T = 10^4 K$  in

these models. S08 and K08 apply this criterion to the halo virial temperature, while MORGANA takes into account the temperature profile of the hot halo gas. In reality, of course, cooling via molecular hydrogen allows gas to cool down to lower temperatures, and would permit cooling in haloes with  $T < 10^4 K$ . K08 and S08 adopt fairly standard versions of the cooling model proposed by White & Frenk (1991), whereas MORGANA adopts a somewhat modified version of this model presented in Viola et al. (2008).

In all three SAMs, once gas is “cold” it can be converted into stars on a timescale that is given by some form of Schmidt-Kennicutt law. The size of the galactic disc is estimated using angular momentum conservation arguments, and this size is used to estimate the gas surface density that enters the Schmidt-Kennicutt expression (we refer interested readers to the original papers for more details).

Massive stars and supernovae may impart thermal and kinetic energy to the cold interstellar medium, and reheat the cold gas or drive winds that eject gas from the halo. In the K08 and S08 models, the rate of reheating of cold gas is given by an expression of the form:

$$\dot{m}_{rh} = \epsilon_0^{SN} \left( \frac{V_{disk}}{V_0} \right)^{\alpha_{rh}} \dot{m}_* \quad (2)$$

where  $\epsilon_0^{SN}$  and  $\alpha_{rh}$  are free parameters and  $\dot{m}_*$  is the star formation rate. K08 and S08 adopt similar values of  $\epsilon_0^{SN}$  and  $\alpha_{rh} \sim -2$ , chosen to reproduce the faint end slope of the observed  $z = 0$  global galaxy luminosity function or the low-mass end of the stellar mass function.

The supernova feedback recipe in the original MORGANA model, as published in Monaco, Fontanot & Tafoni (2007), implements a recipe calibrated on the results of Monaco (2004) and based on the notion of a self-regulated feedback loop between star formation and supernovae. In this prescription the reheating rate (Eq. 2) is always equal to the star formation rate (ejection from the DM halo through superwinds is regulated by the dynamics of the hot halo component), so that  $\epsilon_0^{SN} = 1$  and  $\alpha_{rh} = 0$  in terms of Eqn. 2, above. With this prescription, MORGANA reproduces many properties of relatively massive galaxies ( $M_* > 10^9 M_\odot$ ). However, we find that in order to reproduce the MW satellite LF with MORGANA we need to introduce a strong dependence of the mass loading factor  $\eta \equiv \dot{m}_{rh}/\dot{m}_*$  on the galaxy circular velocity:  $\alpha_{rh} = -4$  (see Sec. 5.4.3 for more details). In order to avoid degrading the agreement on larger mass scales, we retain the original feedback model in DM haloes with  $V_c > 100$  km/s and adopt Eqn. 2 in galaxies in haloes  $V_c < 100$  km/s. In the present context we prefer not to give a physical justification for this choice but only a phenomenological one: the standard version of MORGANA fails in predicting the LF of MW satellites, but adopting the commonly used differential scaling of  $\eta$  with circular velocity (though with a stronger scaling exponent) solves this problem. Whether it is physically correct or not remains to be seen, but clearly this phenomenological scaling is a partial key to the success of galaxy formation models in the  $\Lambda$ CDM context in predicting the MW satellite LF.

In all three models, the production of heavy elements (metals) is tracked using a simple chemical evolution model based on the instantaneous recycling approximation, in which the effective yield  $y_{eff}$  is treated as a free parameter. Metals are initially deposited in the cold gas, but may

be heated and mixed with the hot halo gas or ejected from the halo by supernova feedback.

Finally, in order to compute observable quantities such as magnitudes and colors, the predicted star formation and enrichment histories are convolved with simple stellar population (SSP) models. K08 and S08 use the Bruzual & Charlot (2003) SSP models, while MORGANA makes use of the stellar population models incorporated within the GRASIL code (Silva et al. 1998). All the models used in this work adopt a Chabrier stellar initial mass function (Chabrier 2003).

All three models also account for the attenuation of stellar light due to dust extinction. In K08 and S08, simple analytic models for dust extinction are adopted, while MORGANA is interfaced with the GRASIL code (Silva et al. 1998), which contains a radiative transfer solver to account for dust attenuation and re-emission (see Fontanot et al. 2009 for a quantitative comparison between the prediction of radiative transfer solvers and analytic prescriptions for dust attenuation). However, dust extinction has a negligible impact on the predicted magnitudes and colors of the very small, faint dwarf galaxies that we focus on in our study, because of the low metallicities and gas contents of these objects. Therefore we do not expect these differences in the modelling of dust to significantly impact our results.

It is worth noting that the ingredients of these SAMs have all been developed with much larger galaxies in mind, and the models have previously been calibrated mainly against observations of relatively luminous galaxies ( $M_* \gtrsim 10^9 M_\odot$  or  $M_V \lesssim -16$ ). It is quite unclear whether the standard semi-analytic empirical recipes for e.g. star formation or supernova feedback should apply in galaxies as tiny as the ultra-faint Milky Way dwarfs, which may form out of just a few molecular clouds. Therefore, it is quite an interesting experiment to see how well these models perform when extended to these very different mass scales.

#### 4 OBSERVATIONAL DATA

We test our MW models against observations by focusing on three key aspects of MW satellite galaxy properties: their luminosity, stellar mass, and radial distributions.

For the luminosity function we use the results of Koposov et al. (2008; SK08 hereafter). SK08 recently presented a quantitative search methodology for Milky Way satellites in the SDSS DR5 data and used this method to compute detection efficiency maps, which ultimately allowed the construction of the first completeness-corrected satellite galaxy luminosity function (see also Walsh, Willman & Jerjen 2009). SK08 measured the luminosity function (LF) down to  $M_V = -2$ , and found that it can be described by a single power law of the form  $dN/dM_v = 10 \times 10^{0.1(M_V + 5)}$ . At the very faint end ( $M_V > -5$ ), in order to compute the completeness correction, a radial satellite distribution around the host must be assumed; in all the luminosity function plots presented in this paper the upper data points (always shown as open circles with no error bars) are obtained assuming an isothermal density distribution while the lower points (solid circles with error bars) are obtained assuming an NFW (Navarro, Frenk and White 1997) distribution.

We also use a reverse approach to addressing the completeness issue by performing the comparison in “observa-

tional space”. Instead of assuming a radial distribution for the observed galaxies, we apply the detection criteria of the SDSS to our simulations (see section 5.3 for more details) and compare directly with the raw data from the SDSS. For this comparison we construct a “hybrid” data set. For satellites brighter than  $M_V = -10$ , in order to increase the number statistics, we gather together satellites from the Milky Way and the Andromeda galaxy (data from Mateo 1998 and Metz et al. 2007), and we assign a weight of  $w = 0.5$  to each satellite, assuming that current surveys are complete down to this limit. For fainter satellites we collect data from Martin, de Jong & Rix 2008 (MdJR08 hereafter) and, in order to account for the fact that the SDSS surveyed only one-fifth of the sky, we set  $w = 5$  for these faint galaxies. The adopted  $M_V$  threshold for splitting the observational sample is justified by the low luminosity of all newly discovered satellites both around the Milky Way and the Andromeda galaxy (McConnachie et al. 2008).

In addition, using the same data set described above, we compute the cumulative radial distribution of satellites (i.e. the number of satellites within a given distance from the Sun). Distances for bright satellites are taken from Metz et al. (2007), while we use results compiled in MdJR08 for faint galaxies ( $M_V > -10$ ). In computing the radial distribution we assign to each galaxy the same weight adopted for the LF. The stellar mass function is derived from the SK08 luminosity function under the assumption that satellites have a mass-to-light ratio of unity in solar units in the V band. This relation holds for both faint (MdJR08) and luminous galaxies (Bell et al. in prep.). Figure 1 shows the differential stellar mass function of Milky Way satellites that we derived, and the dotted line is the equivalent of the power law found by SK08 to describe the luminosity function. Error bars represent the Poisson scatter in each bin. In our comparison with the simulations, we adopt the NFW radial distribution in computing the cumulative stellar mass function from the data.

#### 5 RESULTS

In this section we present results for both the SAMs and numerical (dissipational and dissipationless) simulations and compare them with the observational data set described in Section 4. First we compare the dynamical evolution of satellites in SAMs and in N-body simulations, and then we present results for the Luminosity Function (LF) of simulated satellites and analyze the importance of different physical processes (e.g. reionization, stellar stripping and supernova feedback) in shaping the LF. We then present results for the stellar mass function and the radial distribution and how they compare with observations.

##### 5.1 Dynamical evolution of sub-haloes in SAMs and N-body simulations

In the SAMs investigated here, we chose to make use of N-body based merger trees for “isolated” (or distinct) haloes only, and to model the dynamical evolution of satellites semi-analytically (see Section 3). Thus, there will not be a one-to-one correspondence between the masses or positions of sub-haloes at  $z = 0$  in the SAMs and in the actual

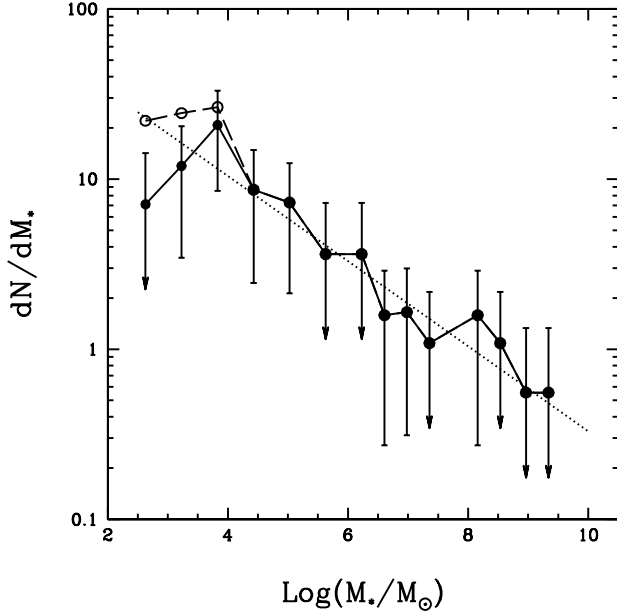


**Figure 1.** The stellar mass function of observed Milky Way satellite galaxies, obtained from the SK08 determination of the satellite luminosity function, assuming  $L_V/L_{V,\odot} = 1M_*/M_\odot$  for all satellites (see text for more details). Solid symbols show results inferred assuming an NFW-like radial distribution, open circles are for an isothermal distribution. The arrows on error bars indicate that there is only one galaxy in that particular bin, and so the Poisson error is formally 100%.

N-body simulations. In this section we check that the statistical distributions of subhalo masses and radii predicted by the semi-analytic models are in agreement with those of subhaloes identified in the N-body simulations. This comparison is only possible for the K08 and S08 models, since the MORGANA model does not explicitly follow the dynamics of dark matter substructures. Figure 2 shows the cumulative subhalo mass function from N-body and SAMs for our four Merger tree G0-G3. The G1<sub>HR</sub> halo is shown for the K08 model only. The SAM results are obtained by averaging over 10 different realizations of the random orbit selection process and are truncated at the N-body mass resolution limit. Both the K08 and S08 SAMs produce good agreement with the subhalo mass function from the N-body at low and intermediate masses; at high masses the SAMs tend to predict slightly too many surviving subhaloes.

The radial distribution of satellites is a key piece of information for deciding whether a satellite will be detectable in the SDSS survey. It is therefore important to also check that the SAMs correctly predict the radial distribution of subhaloes within the parent halo. Figure 3 shows the radial number density of subhaloes (without including the central galaxy); also in this case there is a good agreement between SAMs and N-body results for both models.

In the semi-analytic models used here, the initial orbit eccentricity of an infalling subhalo is randomly selected from a distribution motivated by the results from cosmological N-body simulations. The orbit eccentricity affects the dynamical friction time scale (radial orbits merge more rapidly than circular orbits). In figure 4, we show the radial distribution

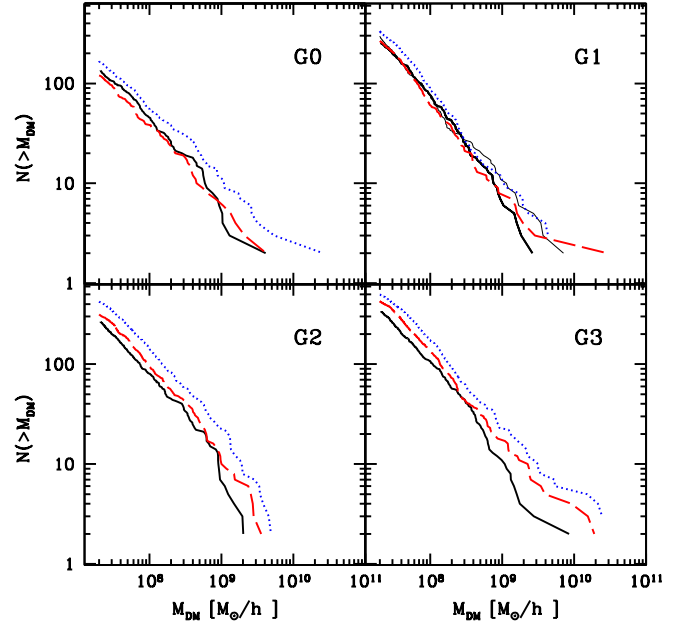


**Figure 2.** Comparison between the subhalo mass function at  $z = 0$  (within  $R_{\text{vir}}$ ) in the N-body simulations (solid black line) and the predictions from the semi-analytic models of K08 (red dashed line) and S08 (blue dotted line). Each panel shows results for a different dark matter halo. The (black) thin solid line in the G1 panel shows the results of the K08 SAM when applied to the G1<sub>HR</sub> halo.

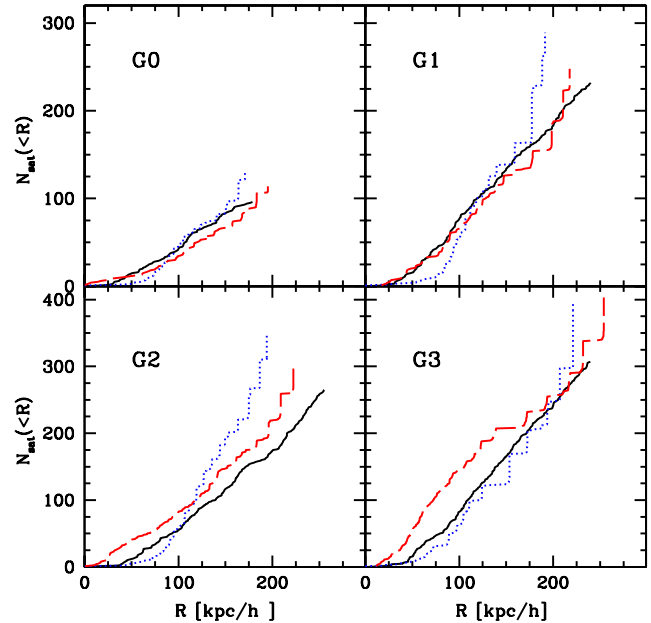


**Figure 3.** The cumulative radial number density of satellites. The results from the N-body simulations are shown by the solid (black) line, and results from the K08 and S08 SAMs are shown by the (red) dashed line and (blue) dotted line respectively. Each panel shows results for a different dark matter halo.

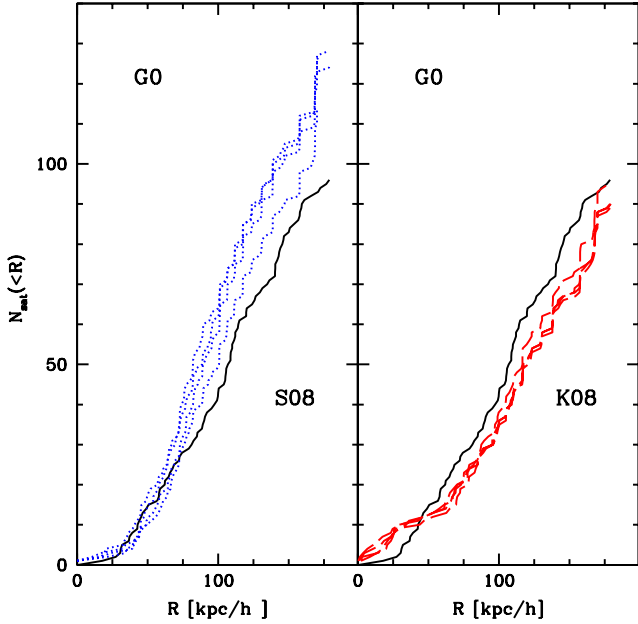


**Figure 4.** The effects of orbit selection on the satellite radial distribution. Each panel shows four different realizations of the random orbit selection process for the G0 halo. The N-body simulation results are shown by the solid (black) line, and results from the S08 and K08 models are shown by the (blue) dotted and (red) dashed lines on the left and right panels respectively.

function of subhaloes for four different realizations of the random orbit selection process. We can see that the scatter due to different realizations of the orbit distribution is fairly small, and mostly effects the less numerous, massive satellites which are not the focus of our study.

## 5.2 Satellite Luminosity Function

We now compute satellite LFs using the 4 merger trees obtained from the N-body simulations as common input for our semi-analytic models; this allows us to isolate the impact of the different physical ingredients in the SAMs because the DM halo merger histories are exactly the same in all three models. Figure 5 shows the predictions from our three SAMs, adopting  $z_r = 7.5$  as the redshift of reionization. We plot all satellites within  $R = 280$  kpc in order to be consistent with the SK08 data set. Solid lines show the mean of satellite distribution and the (grey) shaded area shows the  $1\sigma$  Poisson scatter around that mean.

All of the models predict that the number of satellites brighter than  $M_V = -3$  is of the order of  $\sim 100$  and could easily be several hundreds (e.g. G3). This is in agreement with recent estimates of the number of observed satellites obtained by several different approaches (e.g. Tollerud et al. 2008; Madau et al. 2008; Koposov et al. 2009);

All the models show that the total number of satellite galaxies depends on the host halo mass. The LF of the G0 halo (the least massive one, see Table 1) is almost flat and has a lack of satellites at the faint end compared to the MW data. On the other hand, in the most massive halo (G3), the SAMs predict more satellite galaxies at all luminosities than

are observed in the MW. This trend between halo mass and the LF does not depend on the SAM used to populate dark matter substructures and indicates that the total mass of the dark matter halo has a quite strong influence in determining the normalization (and shape) of the satellite LF.

All three semi-analytic models considered in this work are able to do a reasonably good job of reproducing the observational data. The K08 and S08 models (upper and middle panels) in figure 5 quite successfully reproduce the observed LF for satellite galaxies over the entire luminosity range  $-2 \geq M_V \geq -16$ . The MORGANA model (lower panels in figure 5), tends to predict slightly more satellites at intermediate luminosity ( $-10 > M_V > -12$ ) but it is nonetheless in good agreement with the observations especially if an NFW distribution is assumed for observed satellites. In the G1 panel for the K08 model we also show the LF obtained using the G1<sub>HR</sub> merger tree (dotted black line). We see that the higher resolution merger tree produces almost indistinguishable results. We also tested the effect of the random orbit selection on the satellite luminosity function; as already shown for the radial distribution (see figure 4) the effect of the orbit selection has a negligible effect on the faint end and only marginally changes the slope of the LF at the bright end.

In some cases, certain models and certain haloes show a dearth or even absence of the most luminous satellites (e.g. S08 and K08 G0, G2 in all models). This should not be a serious cause for concern, because the variance in the number of massive subhaloes hosting these luminous satellites is very large and depends on the detailed merger history of the halo. Moreover, the predicted number in the SAM is very sensitive to the random orbit chosen, as discussed in Section 5.1. To more assess this issue in a more robust way, we need to increase the number of merger tree realizations of MW mass haloes. We do this using semi-analytic merger trees instead of the merger trees extracted from N-body simulations. For each model we generated 40 merger trees for DM haloes in the supposed mass range of the Milky Way dark matter halo,  $(0.8 - 1.2) \times 10^{12} h^{-1} M_\odot$  (Klypin, Zhao & Somerville 2002). Each of the SAM codes has its own algorithm for generating merger trees: the K08 and S08 model use different implementation of the EPS algorithm, while MORGANA uses the PINOCCHIO code (see Section 3). Figure 6 shows the averaged luminosity function for the three semi-analytic models (we tested that the sub-halo mass function from the EPS/PINOCCHIO trees is in agreement with the one extracted from the Nbody simulations).

The K08 and S08 model are, again, in good agreement with the observational data: they are able to fit the Milky Way luminosity function in the range  $-15 < M_V < -2$ . The K08 model shows a small deficit of satellites at brighter magnitudes (especially if compared with S08 and MORGANA) but this occurs where the number of observed satellites has a large error bar due to poor number statistics. Our models produce much better agreement with the number of luminous satellites with  $M_V < -15$  relative to the predictions of Benson et al. (2002). Because of the large number of differences between the Benson et al. models and those considered here, we can only speculate on the source of this difference.

It is also interesting to note that the K08 and S08 models suggest that the LF of ultra-faint satellites has a downward kink below about  $M_V \sim -6$ , in better agreement with



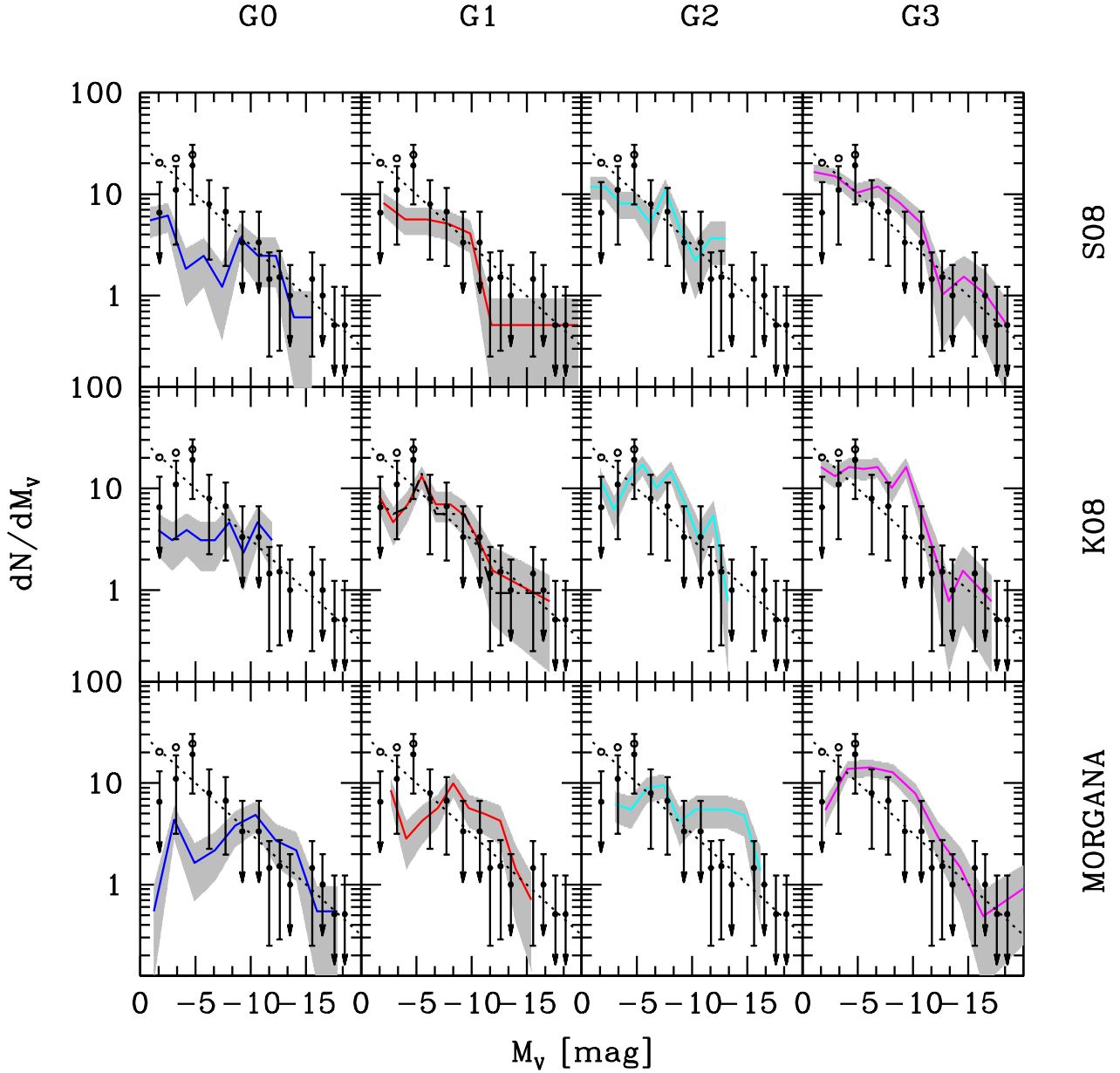


**Figure 5.** The Milky Way satellite luminosity function predicted by our three semi-analytic models (S08, K08 and MORGANA from top to bottom) using the G0-3 halo merger trees (from left to right), with an assumed reionization redshift  $z_r = 7.5$ . The median of the satellite distribution is shown by the solid line, while the shaded area represents the  $1\sigma$  Poisson scatter around the mean. Observational data are taken from SK08 under the assumption of two different radial distributions of satellites, NFW-like (solid circles with error bars) and isothermal (open circles). The arrows on error bars indicate that there is only one galaxy in that particular bin, and so the Poisson error is formally 100%. The dotted line shows a single power law fit to the data:  $dN/dM_v = 10 \times 10^{0.1(M_V + 5)}$ . In the G1 panel of the K08 model results for the G1<sub>HR</sub> run are also shown as a dashed (black) line.

the SK08 observational results adopting an NFW, rather than isothermal, radial density distribution for the satellites. An NFW distribution for satellites is predicted by hydrodynamic simulations (Macciò et al. 2006). The comparison between the MORGANA model and the observational results can only be performed down to  $M_V = -5$  in this case. This because the PINOCCHIO code has never been tested on such small scales (e.g. Li et al. 2006) and we did not feel

confident in using merger trees with a mass resolution below  $\sim 10^8 h^{-1} M_\odot$ . In the tested range for  $M_V$  the MORGANA model is also in good agreement with observations.

In figure 7 (lower panel) we plot the stellar mass and luminosity of galactic satellites versus their dark matter subhalo mass; results are shown for the K08 model for all haloes, and are similar for the other models. For this comparison we used both the present dark matter mass

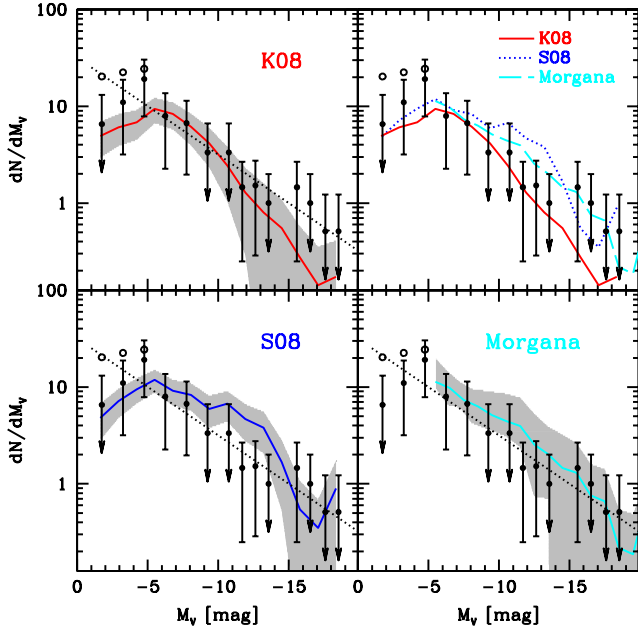


**Figure 6.** Satellite Luminosity function predicted by SAMs using semi-analytic merger trees (EPS and PINOCCHIO, see text for details). Symbols have the same meaning as in figure 5. The upper right panel shows the average satellite LF for the three semi-analytic models together. MORGANA results are shown only down to  $M_V = -5$ , due to a resolution limitation in the PINOCCHIO code; see text for more details.

( $M_{DM}(z=0)$ ) and the mass of the subhalo at the time of accretion ( $M_{DM}(z_{acc})$ ). The difference between the two reflects the effects of tidal stripping on the dark matter substructure. The correlation between the present day dark matter mass and luminosity is quite broad and, for low luminosities,  $M_{DM}(z=0)$  at a fixed luminosity spans almost 3 orders of magnitude. This is because tidal stripping of the dark matter subhalo washes out the initial correlation between luminosity and  $M_{DM}(z_{acc})$ . The same applies to the comparison between the dark and stellar mass of galactic satellites, as shown in the upper panel of figure 7.

Recently, Strigari et al. (2008) pointed out that one of the curious properties of the newly discovered population of ultra-faint satellites is that over four orders of magnitude in luminosity, these objects seem to contain a nearly constant total mass within a radius of 300 pc. If we focus on the ultra-faint population in figure 7, with  $-3 < M_V < -10$ , we can see that the huge scatter in DM mass at fixed luminosity or stellar mass provides a partial explanation for this apparent “common” mass scale for the ultra-faint satellites. Macciò, Kang & Moore (2009) investigated this in more detail, and presented a direct comparison between the predicted luminosity and the mass within 300 pc for ultra-faint satellites in our simulations. They argued that the inner profiles of haloes that are initially very concentrated are less affected by tidal heating than haloes that are less concentrated, so that the mass within 300 pc is reduced for more massive subhaloes (which are less concentrated) relative to less massive ones. When they corrected for this concentration-dependent modification of the inner density profile, they found that the

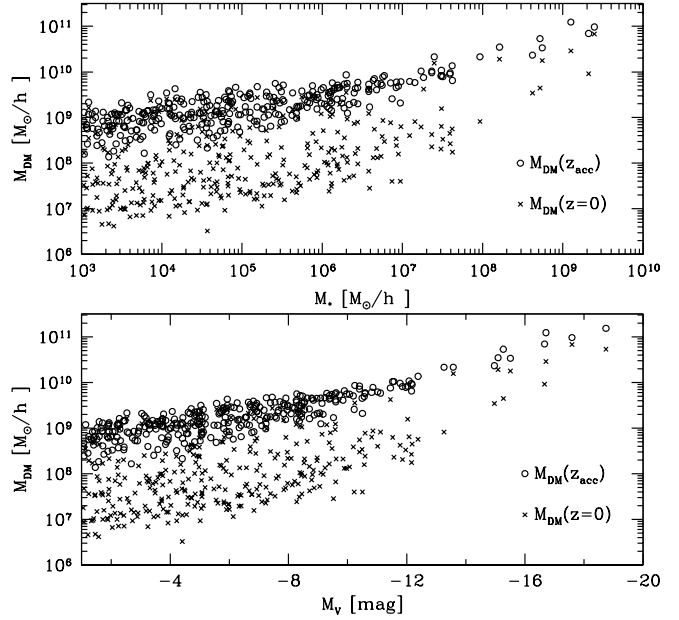


**Figure 7.** The dark matter mass of galaxy satellites versus their luminosity (lower panel) and stellar mass (upper panel). Open circles show the masses at time of accretion, while crosses show the present ( $z=0$ ) dark matter mass. Results are shown for the K08 model for all haloes G0-G3.

Strigari et al. (2008) results are quantitatively reproduced by our simulations.

### 5.3 Luminosity Function in the Observational Plane

The luminosity function of SK08 has been determined under certain assumptions for the radial distribution of satellites around our Galaxy. It is also interesting to apply the observational selection criteria to our simulations and compare “in the observational plane”, i.e. with the *raw* data from the SDSS without completeness corrections applied. To make such a comparison we have applied to our sample of satellites a *visibility* criterion, in order to determine if a given satellite would be detected in the SDSS. We assume that *all* satellites brighter than  $M_V = -10$  would be visible and included in the SDSS sample. For fainter satellites, we adopt a criterion based on both satellite distance and luminosity (see SK08 for more details):

$$\log(R/\text{kpc}) < 1.04 - 0.228 \times M_V. \quad (3)$$

In the above formula the distance  $R$  is measured from the Sun and not from the center of the galaxy. In order to convert our galacto-centric distances into helio-centric distances, we assume the Sun to be located at 8 kpc from the center of the galaxy (8,0,0); moreover, since for each satellite galaxy we only know its distance from the galactic center, we randomly assign position angles  $(\phi, \theta)$  to each of them (see also Tollerud et al. 2008). We exclude from the comparison galaxies more distant than 280 kpc. Moreover since the SDSS covers only approximately one fifth of the sky we randomly select 1/5 of our satellites. We then average over 100 different realizations of this random sampling. Obser-

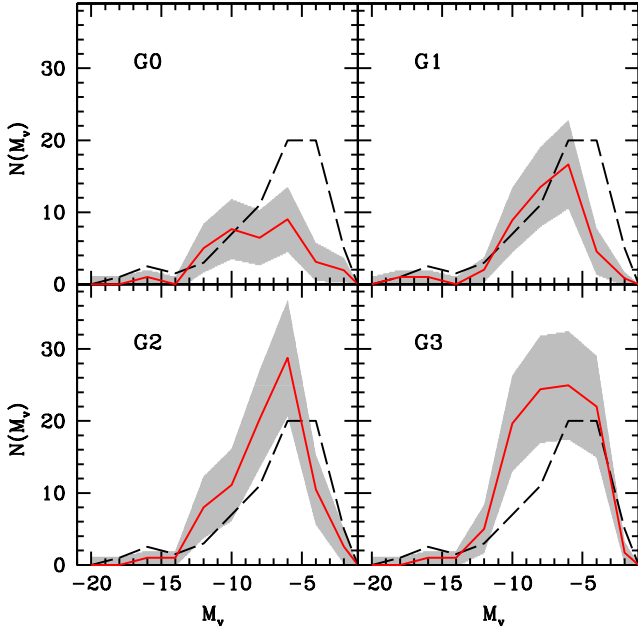


**Figure 8.** Comparison between the “raw” SDSS data (uncorrected for completeness) and model predictions with the SDSS visibility criteria applied to the simulations (see text for details). The observational data are shown by the (black) dashed line, the K08 model is shown by the solid (red) line, and the shaded area shows the  $1\sigma$  Poisson scatter around the mean value.

observational data for the recently discovered SDSS satellites are taken from MdJR08. Figure 8 shows the comparison between the observations and the luminosity functions obtained with the K08 model (the S08 model gives very similar results and this comparison is not possible for the MORGANA model, because it does not provide the distance of satellite galaxies from the main halo). The direct comparison with the observational data confirms our previous results on the luminosity function. Our models are able to reproduce the data for haloes G0-G2, while halo G3 slightly overproduces the number of faint satellites. The agreement between the data and models implies that the distance-luminosity relation of our satellites is similar to the observed one.

The application of the selection criteria of the SDSS to our simulated data also allows us to compare the radial number density of satellites in our models *vs* observations. Results are shown in figure 9. From this figure we see that our simulations reproduce both the observed slope and normalization of the satellite radial distribution.

Finally in figure 10 we compare the radial distribution of DM substructures and “observable” satellites in the K08 model (obviously, observability depends on many factors, but in this context we simply consider all satellites with  $M_V < -1$  to be “observable”). In the upper panel we show the number density radial distribution of all “observable” satellites ( $M_V < -1$ ), of ultra-faint satellites ( $-9 < M_V < -1$ ) and of classical satellites ( $M_V < -9$ ). The number-weighted distribution of observable satellites (which are dominated by the much more numerous ultra-faint population) traces the sub-halo distribution (but is down by a factor of  $\sim 2$ ) at small radii (within  $R/R_{\text{vir}} \approx 0.2$ ), but flat-

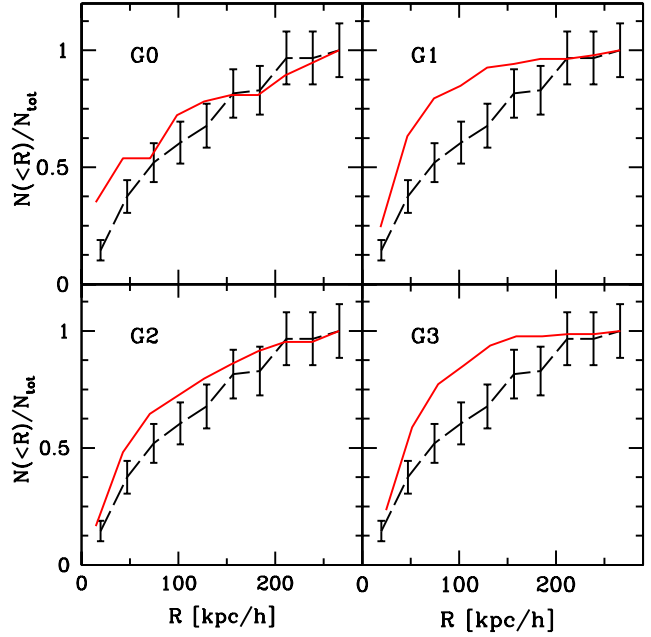


**Figure 9.** The fraction of satellites as a function of the distance from the central galaxy. Observational data are shown by the (black) dashed line with error bars (representing the Poisson noise). The K08 model is shown by the solid (red) line.

tens relative to the sub-halo distribution at large radii. This implies that “observable” sub-haloes are more concentrated near the large galaxy than the overall population of sub-haloes (see also Kravtsov et al. 2004). When satellites are weighted by their mass (lower panel of the same figure), the distribution is dominated by the classical (bright) satellites, and is almost identical to the mass-weighted distribution for all sub-haloes. Thus, the different radial distribution of “observable” and dark satellites is due to the suppression of star formation in low-mass haloes due to cosmic reionization and feedback processes.

#### 5.4 Physical Processes that Shape the Satellite Luminosity Function

We have shown that it is indeed possible to reproduce the observed Milky Way satellite luminosity function within the  $\Lambda$ CDM model; we now investigate the role of various physical processes in shaping the LF in our theoretical models, with a focus on the origin of the ultra-faint satellite population. There are several possible physical origins for the ultra-faint satellite population: it can originate from (i) object that formed in haloes with  $T < 10^4$  K via  $\text{H}_2$  cooling; (ii) haloes with  $T > 10^4$  K that were inefficient at accreting (hot) gas, because of photoionization; (iii) haloes with  $T > 10^4$  K in which star formation was inefficient because of strong supernova feedback; (iv) objects that originally had larger stellar masses but have experienced significant stellar stripping.

In the following sections we will investigate scenarios (ii)-(iv). The first scenario, in which the ultra-faint dwarfs form via  $\text{H}_2$  cooling in haloes with  $T < 10^4$  K, is not accounted for in our models. It is likely however that some

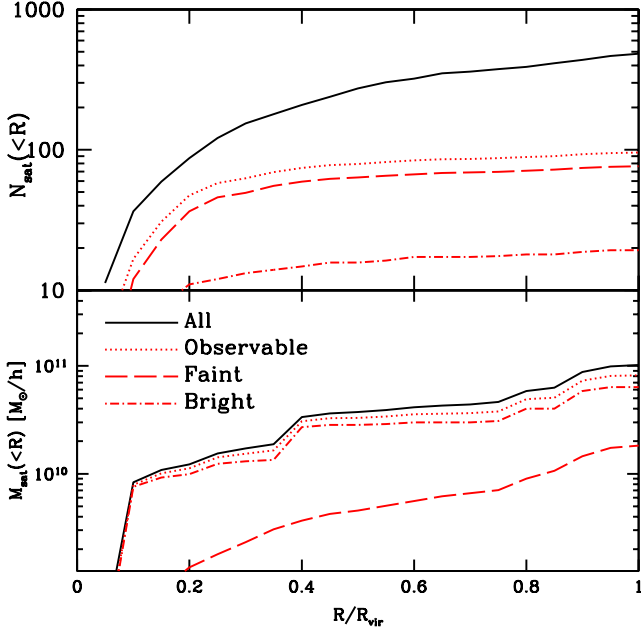


**Figure 10.** Upper panels: number-weighted cumulative fractional radial distribution of satellites; the black line shows all substructures (dark and observable), the (red) dotted, dashed and dot-dashed lines are for the “observable” satellites ( $M_V < -1$ ), the ultra-faint satellites ( $-9 < M_V < -1$ ) and the classical satellites ( $(M_V < -9)$ ), respectively. Lower panel: same as upper panels but with weighted by satellite mass. The results were obtained by averaging over the four haloes G0-G3; only the K08 model is shown.

ultra-faint satellites could form in this way, and this could help in explaining the small gap between the theoretical predictions and observations for  $M_V \gtrsim -3$  (e.g. figure 6).

#### 5.4.1 Reionization

We test the effect of our adopted parametrization of cosmic reionization on our results, by both varying the reionization redshift within our reference model based on Kravtsov et al. (2004) and by applying a simple modification to this model to take into account recent results based on high resolution hydrodynamical simulations (e.g. Okamoto et al. 2008; Hoefft et al. 2006).

The redshift at which reionization occurs is still quite uncertain, but it is bracketed in the range  $7 < z_r < 15$  ( $3\sigma$  range from Komatsu et al. 2009); moreover, due to the fact that reionization proceeds in an inhomogeneous way, the actual redshift of reionization for the Local Group could substantially differ from the average reionization redshift of the Universe (Weinmann et al. 2007). Figure 11 shows the impact of varying the reionization redshift on the G1 luminosity function for the K08 model using the standard reionization parametrization (S08 and MORGANA show a similar trend). Without any suppression of gas accretion due to reionization, the simulated LF contains too few satellites fainter than  $M_V = -5$  and too many with  $M_V \sim -9$ . This is because, in absence of reionization, hot gas can cool very efficiently via atomic cooling, and every halo can transform a large fraction of its gas content into stars before SN feedback shuts star formation down. When the effect of reioniza-

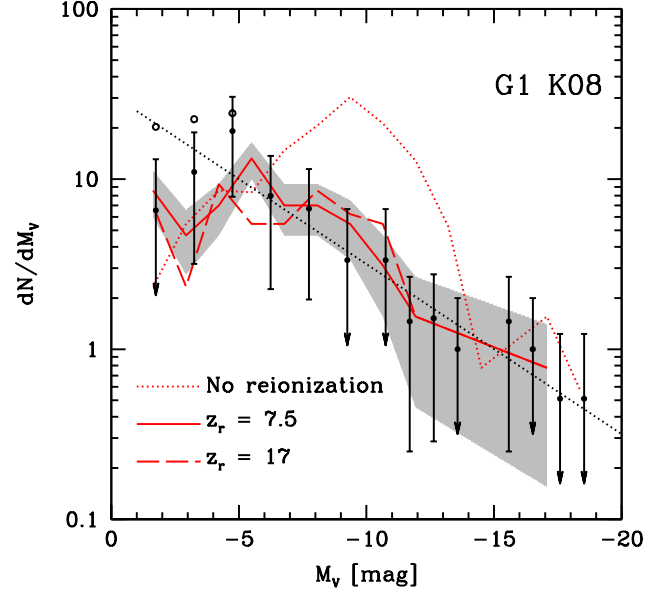


**Figure 11.** Satellite luminosity function of the G1 halo in the K08 model for three different reionization redshifts. The solid line represents our fiducial model with  $z_r = 7.5$ , the dashed line is for  $z_r = 17$ , and the dotted line is for a model with no reionization (but including all other kinds of feedback). The shaded area represents the  $1\sigma$  scatter around the mean of the  $z_r = 7.5$  model.

tion is taken into account, the amount of gas available for cooling and star formation is reduced in low mass haloes, and many galaxies are shifted from intermediate luminosities ( $-15 < M_V < -6$ ) to low luminosities ( $M_V > -6$ ), producing a luminosity function that is close to a power-law and is in good agreement with the data. It is also interesting to note that the LF is almost insensitive to the redshift of reionization (solid line shows results for  $z_r = 7.5$ , dashed line for  $z_r = 17$ ); this is in agreement with earlier results obtained by Kravtsov et al. (2004).

In addition to uncertainty about the redshift of reionization, there is still a debate about the value of the characteristic mass,  $M_F$ , below which galaxies are strongly affected by photoionization. Okamoto et al. (2008, see also Hoefft et al. 2006), using hydrodynamical simulations, recently suggested that the actual value of  $M_F$  can be significantly lower than values previously obtained (e.g. by Gnedin 2000). In order to explore the implications of their results, we introduce a factor  $\gamma$  that multiplies the original value of  $M_F(z)$  as derived by Gnedin (2000, see eq. 1). We have used two constant values for  $\gamma$ , namely 0.2 and 0.5, and a redshift dependent expression  $\gamma(z) = (1+z)^{1.1}/11.8$ , derived from figure B1 of Okamoto et al. (2008). The results for these three modified models are shown in figure 12 for the G1 halo and for the K08 model (results from the other models are similar). We see that the reduced value of  $M_F$  has the effect of increasing the number of galaxies with  $M_V \sim 10$ , creating a bump in the LF, with respect to the standard case, similar to what we saw in figure 11 for the no reionization run (dotted line). This is true especially for strong suppression of photo-ionization as in the  $\gamma = 0.2$  and  $\gamma(z)$  cases. Nev-

ertheless it is still possible to reconcile the simulated LF's with the observational data by increasing the reionization redshift, as shown in the right panel of figure 12, where we use  $z_r = 11$ .

In summary, it is interesting to note the interplay between the strength of the suppression of gas accretion due to photo-ionization (as reflected in the filtering mass scale) and the redshift of reionization. In our standard models, in which the suppression is relatively strong ( $M_F$  is large), we find a weak dependence of the predicted LF on the adopted value of the reionization redshift, while in models with a lower overall normalization of the filtering mass, we find a stronger dependence on the redshift of reionization.

#### 5.4.2 Stellar Stripping

The MORGANA model allows for the modelling of stellar stripping as a satellite galaxy orbits around the parent galaxy, while the K08 and S08 models assume the stellar content of a satellite to remain unchanged until the dark matter halo is stripped beyond a certain critical point, at which point the galaxy is destroyed completely. Here we investigate the possible effect of stellar stripping on the predicted satellite LF.

In MORGANA, tidal stripping and merging of DM substructures are computed using the Taffoni et al. (2003) fitting formulae, calibrated on  $N$ -body simulations and analytical models. Right after a DM halo merger, the merging and destruction times for the substructure are computed, taking into account dynamical friction, tidal stripping and tidal shocks. Tidal stripping is implemented in MORGANA at a simple level: it is applied at the first periastron of the satellite orbit by computing the tidal radius as the radius at which the density of the unperturbed satellite is equal to the density of the main DM halo at the periastron. All the mass (whether dark, stellar, or gaseous) external to the tidal radius (i.e. at a lower density) is then considered unbound. The MORGANA estimates of the radii of the bulge and disk components, plus assumed density profiles for the stars and gas, are used to estimate the fraction of the baryonic mass that lies outside the tidal radius. The model is applied under the assumption that the density profiles within the tidal radius are not modified by tidal processes.

We compare three different MORGANA runs with no, standard (moderate) and high stellar stripping; this latter case is obtained by increasing by a factor of three the fraction of stripped stellar mass with respect to the standard run (i.e. we remove from the satellites three times the mass that is beyond the tidal radius). Results for the luminosity function are shown in figure 13. In the case of standard stripping the average stripped stellar mass is of the order 5% – 10% with no mass dependence. Comparing the LF of this case with the no-stripping case, it appears that stellar stripping is almost negligible for satellites brighter than  $M_V = -5$  and it marginally affects fainter satellites. When the strength of the stellar stripping is increased the mass loss is, of course, more important and as much as 40% of the stellar mass can be stripped, with a strong dependence on the orbital parameters. However, even in this case the overall effect on the LF is relatively small. According to these results stellar stripping is not one of the most important processes that shapes the satellite LF or produces ultra-faint satellites.

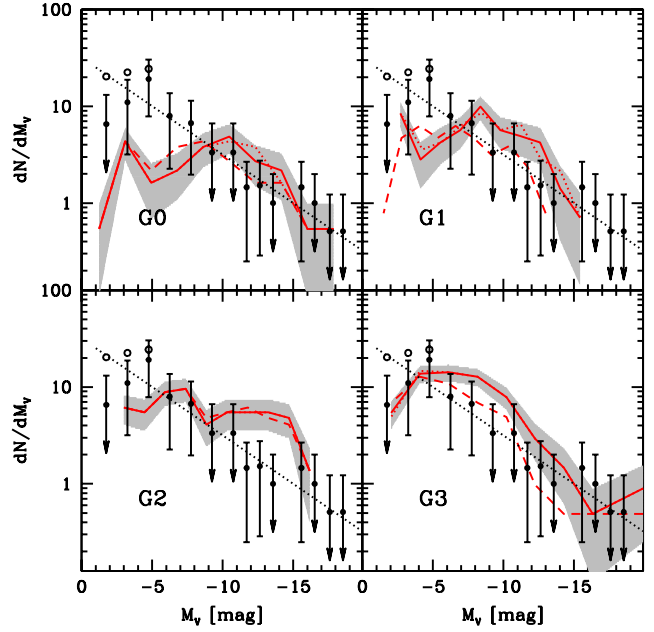


**Figure 13.** The effect of stellar stripping on the satellite luminosity function. Results from the MORGANA model are shown for different levels of stellar stripping (no stripping, standard, and high). The solid line shows the moderate (standard) stripping case (as shown in figure 5); dotted and dashed lines show the no-stripping and strong stripping models respectively.

On the other hand we find that the modelling of tidal destruction of satellites does have a significant effect on the satellite LF. If we neglect tidal destruction, we find many more low-mass subhaloes than are seen in the  $N$ -body simulations, and we would also predict many more faint satellites than are observed in the MW. Figure 14 shows the effect of varying the parameter  $f_{\text{dis}}$  in the S08 model (see sec. 3). Following Zentner & Bullock (2003) and Taylor & Babul (2004), the S08 model considers a satellite to be tidally destroyed when the mass of the dark matter sub-halo has been stripped to a value less than or equal to the mass within  $f_{\text{dis}} r_s$ , where  $r_s$  is the halo's original NFW scale radius. Zentner & Bullock (2003) adopt  $f_{\text{dis}} = 1$  while Taylor & Babul (2004) adopt  $f_{\text{dis}} = 0.1$ . As shown in figure 14, we find good agreement with the observed MW satellite LF for  $f_{\text{dis}} \sim 0.5$ –1.

#### 5.4.3 Supernova Feedback

Feedback from supernovae is believed to be an important mechanism regulating star formation in low mass galaxies and it plays a primary role in shaping the LF in semi-analytic models. It is then important to disentangle its effect from the effect of cosmic reionization discussed in the previous section. To investigate this, we first compare our reference model with both cosmic reionization and SN feedback, and a run with only cosmic reionization (no SN feedback). The results for the K08 model are shown in figure 15; the S08 model shows similar behaviour. In the absence of stellar feedback, the SAM predicts a deficit of faint satellites ( $M_V > -5$ ) and an overabundance of intermediate luminosity satellites ( $-15 < M_V < -10$ ) when compared with the observations. The inclusion of SN-driven outflows

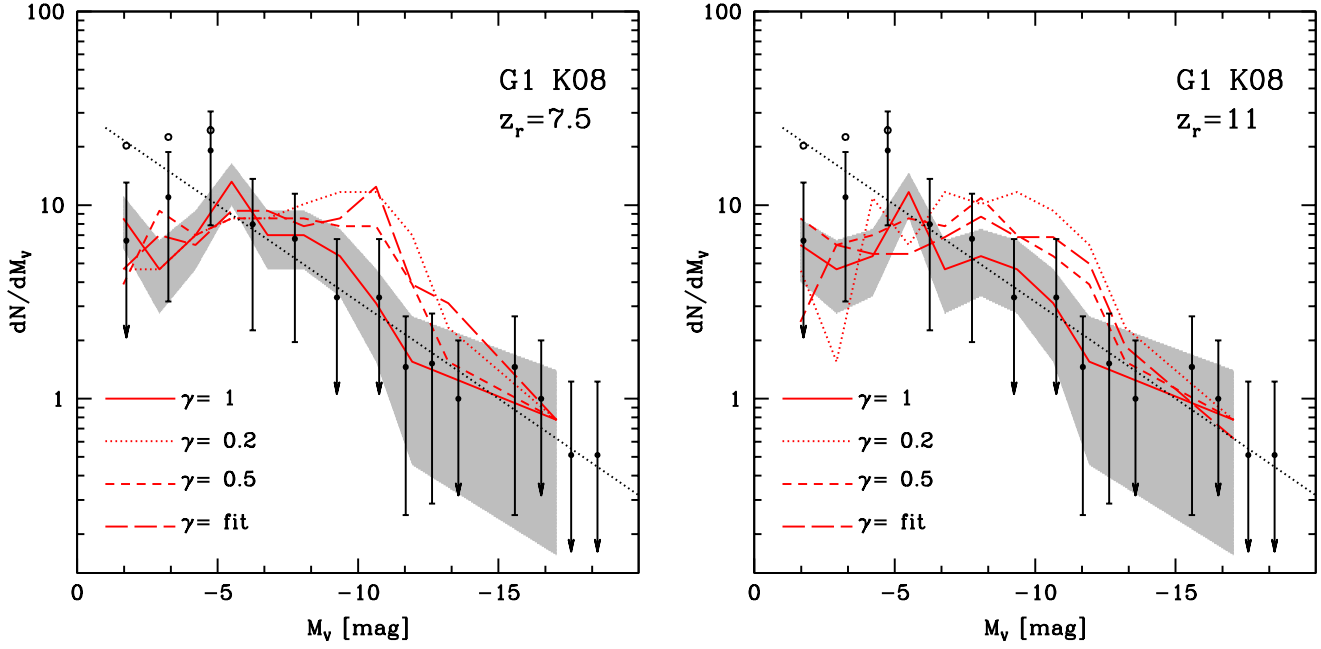


**Figure 12.** Satellite luminosity function for the G1 halo in the K08 model, for different parametrizations of cosmic reionization. The solid line shows results for the standard reionization model ( $\gamma = 1$ , see text for the definition of  $\gamma$ ) based on Kravtsov et al. (2004). The dotted and short dashed lines show results for a filtering mass  $M_F$  reduced by 80% and 50% respectively. The long dashed line is for a model with a redshift dependent expression for the modification of  $M_F$  (see text for more details). The shaded area represents the  $1\sigma$  scatter around the mean of the  $\gamma = 1$  model. The left and right panels are for  $z_r = 7.5$  and 11 respectively.

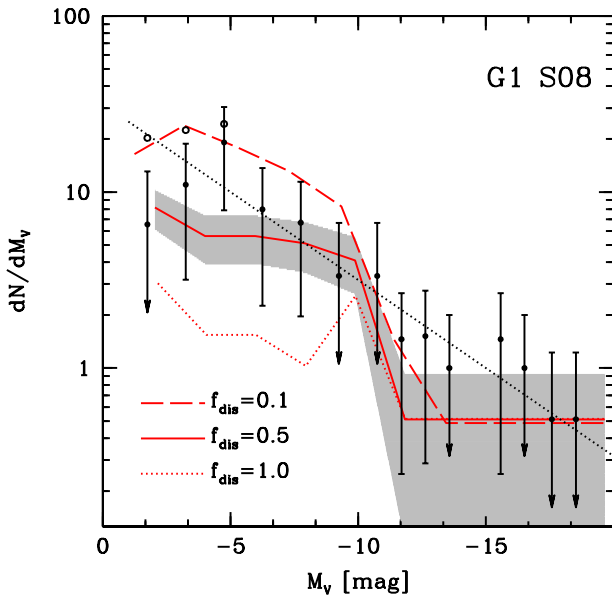


**Figure 14.** The effect of varying the tidal destruction parameter  $f_{\text{dis}}$  (see text) on the predicted MW satellite LF in the S08 model, for the G1 halo.

again moves intermediate luminosity galaxies into the ultra-faint regime by removing a significant fraction of the gas and thereby suppressing star formation.

As we already discussed in Sec. 3 the original version

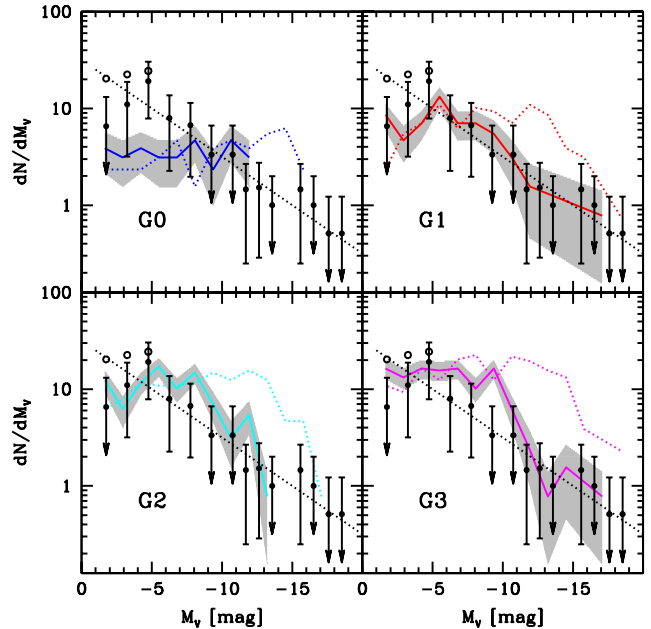


**Figure 15.** The effect of supernova feedback on the satellite luminosity function. Results from the K08 model with SN feedback switched *on* (solid line with shaded area) and *off* (dotted line) are shown.

of the MORGANA model, implementing a recipe for supernova feedback derived from Monaco (2004), does not produce good agreement with the MW satellite LF. In order to reproduce the observed MW satellite LF, we found it nec-



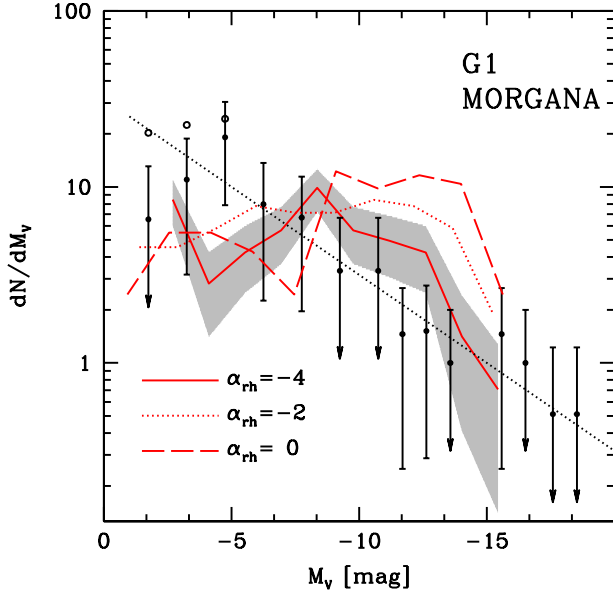


**Figure 16.** The effect of supernova feedback on the satellite luminosity function for the G1 halo in the MORGANA model. Results are shown for the original MORGANA SN feedback recipe (dashed line), and with an intermediate (dotted) and strong (solid) dependence of SN feedback on galaxy internal velocity (see text for details).

essary to modify the stellar feedback modeling using an approach similar to K08 and S08. We compare the predictions of the original and modified models in figure 16. We show both the predictions of the modified model with  $\alpha_{\text{rh}} = -2$  (the reference value in K08 and S08), and with  $\alpha_{\text{rh}} = -4$ .

Thus we conclude that strongly *differential* SN feedback (in which the outflow rate relative to the star formation rate is much higher in low-mass galaxies) plays a key role in reproducing the MW satellite LF in these models.

#### 5.4.4 Satellite Strangulation

There is another effect that in our models can cause relatively high-mass haloes ( $T > 10^4\text{K}$ ) to be inefficient at forming stars and thus to produce ultra-faint satellites. This effect is a result of the fairly standard assumption in SAMs of “satellite strangulation”, namely that the hot gas halo that could provide new gas to a galaxy is stripped immediately when a galaxy becomes a satellite in a larger halo. Thus, haloes that are accreted by the parent halo soon after they crossed the threshold for atomic cooling ( $T > 10^4\text{K}$ ) and thereafter are starved of any new gas cooling or accretion can have very low stellar masses.

In order to explore the importance of this effect, we look for a correlation between satellite luminosity and the timescale  $\tau_S$ , which we define as:

$$\tau_S = \frac{t_{\text{acc}} - t_{\text{form}}}{t_{\text{cool}}} \quad (4)$$

where the formation time ( $t_{\text{form}}$ ) is defined as the time at which the halo reaches a virial temperature  $T > 10^4\text{K}$  and can first begin to cool,  $t_{\text{acc}}$  is the time at which the galaxy is

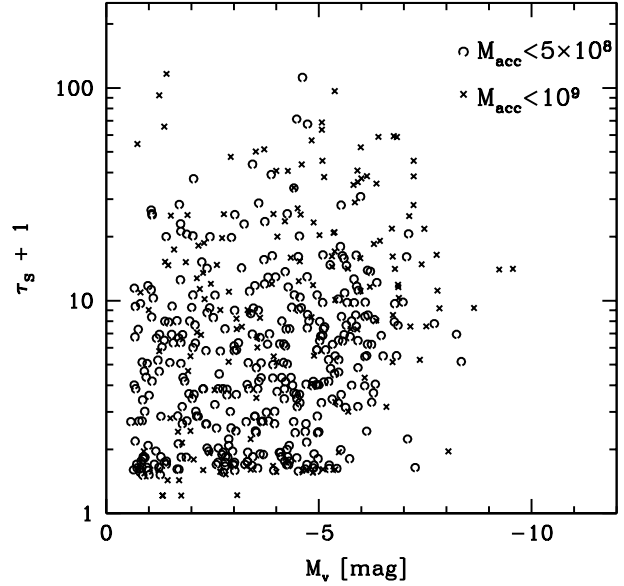


**Figure 17.** Relation between satellite luminosity and  $\tau_S$  (defined according to eq.4) for the K08 model. Different symbols show different values for the total mass of the satellite at the time of accretion, as indicated in the figure label.

accreted by the parent halo and becomes a satellite, and the cooling time ( $t_{\text{cool}}$ ) is the time needed for the gas to radiate away all of its energy via atomic cooling, computed at  $z = z_{\text{acc}}$  (the standard definition of cooling time used in SAMs). Satellites with  $\tau_S < 1$  may have been “strangled” before they were able to cool a significant fraction of their gas. Figure 17 shows that some (about 15 %) of the faint satellites have  $\tau_S < 1$  and therefore may have been impacted in part by this effect (though photo-ionization and SN feedback may still play a role in these objects as well).

#### 5.5 Stellar mass function

We also compare our model predictions with the stellar mass function (SMF) derived from the observations. This allows us to also compare with the results from hydrodynamic simulations, for which we do not have estimates of the galaxy luminosities. The stellar mass functions from the three semi-analytic models are plotted along with the predictions of the hydro simulations and the observational data in figure 18 for haloes G0-G2. The SMF obtained from hydro simulations is in good agreement with the predictions of the SAMs and with the observational data, although unfortunately the comparison cannot be extended to low masses ( $M_* < 10^6 h^{-1} M_\odot$ ) due to the limited mass resolution of the hydro simulations. Nevertheless this represents a success for the GASOLINE code and for its implementation of SN feedback and star formation (see also Governato et al. 2007). The success of the SAMs in reproducing the observationally derived SMF is not surprising given the good agreement we obtained for the LF, nevertheless figure 18 implies that the relation  $L_V/L_{V,\odot} = 1M_*/M_\odot$  is satisfied also for satellites in the semi analytic models.

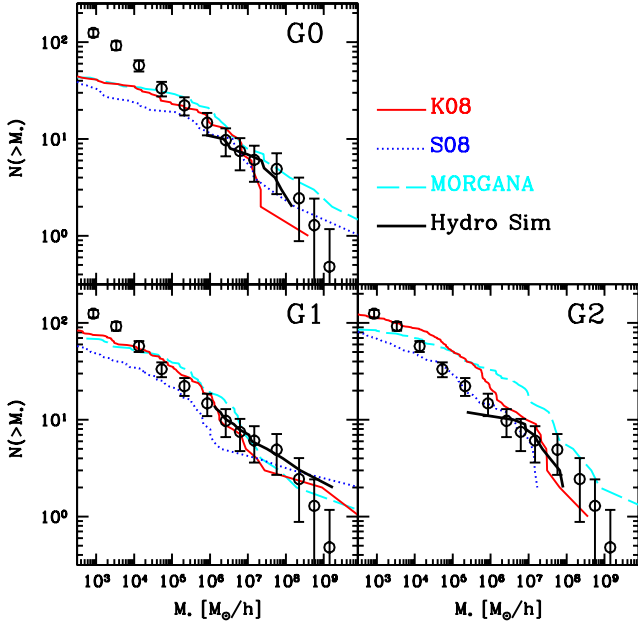


**Figure 18.** The satellite stellar mass function (SMF) from the three SAMs and from hydro simulations for haloes G0-G2, compared with the observationally derived SMF. The K08 model is shown by the (red) long dashed line, the S08 model by the (blue) dotted line, and MORGANA by the (cyan) dot-dashed line. The thick solid (black) line shows the SMF obtained from the hydrodynamic run of each halo (see text for details). Observations are represented by empty circles with error bars.

## 6 DISCUSSION AND CONCLUSIONS

In the last few years, a new population of ultra-faint dwarf satellite galaxies has been discovered around our Galaxy. Given these new observational data, it is timely to revisit the long standing problem of the number of satellites around Milky Way-like dark matter haloes as predicted in the  $\Lambda$ CDM scenario. We address this issue by combining high resolution N-body simulations with three different semi-analytic models of galaxy formation. Four high resolution N-body simulations are used to create detailed merger trees that represent the assembly history of a Galactic dark matter halo. These merger trees are then used as common input for three SAMs for galaxy formation, namely the MORGANA model (Monaco et al. 2007), the Somerville et al. model, (S08, Somerville et al. 2008) and the Kang et al. model (K08, Kang et al. 2008), to study the expected abundance and properties of satellite galaxies in the Local Group.

Because the SAMs do not use the explicit information about subhaloes from the N-body, but track subhalo evolution using semi-analytic recipes, we first compare the mass function and radial distribution of dark matter subhaloes predicted by the SAMs with the results directly obtained from the N-body simulations. We find that the parameterizations of subhalo merging and tidal stripping and destruction adopted by the S08 and K08 models are able to fairly accurately reproduce simulation results for the mass distribution and radial distribution of satellites.

We then test the luminosity function of our simulated satellite population against the latest observational results

for the MW satellite luminosity function. Our models are all able to reproduce the LF down to a magnitude  $M_V = -5$ ; at fainter magnitudes ( $-5 < M_V < -1$ ) the K08 and S08 models also provide a good fit to the observational data, while the MORGANA model tends to underestimate the abundance of ultra-faint satellites, though the predictions are still consistent with the MW data at the  $1\text{-}\sigma$  level. All models seem to suggest a decrease in the satellite number density below  $M_V \sim -5$ , consistent with the assumption of a NFW like radial distribution for observed satellites.

We also perform the comparison between our model predictions and the observations in the “observational plane”, i.e., by applying “visibility” criteria to the simulated satellites and comparing with the SDSS data without any completeness corrections applied. In this case, instead of assuming a radial distribution for the observed satellites (which could in principle depend on e.g. satellite mass or luminosity in a complex way), we make use of the predictions of our models for the joint distribution function of satellite luminosity and distance from the central galaxy. We again find good agreement, increasing the robustness of our results.

We investigated the main physical processes responsible for shaping the luminosity function of Milky Way satellites in our models. In the absence of cooling by molecular hydrogen, and in the absence of processes like photo-ionization, SN feedback, or stellar stripping, the predicted satellite LF would show a peak at around  $M_V \sim -14$  and a sharp drop-off at  $M_V > -10$ , with essentially *no* satellites fainter than  $M_V \sim -8$  predicted. This drop below  $M_V > -8$  is not due to limited numerical resolution, but rather to the sharp assumed cooling cutoff at  $T < 10^4\text{K}$  (because of our adopted atomic cooling function). However, at temperatures just slightly above the atomic cooling cutoff, cooling becomes quite rapid and so in the absence of some kind of feedback or suppression mechanism, these haloes rapidly cool all of the available baryons and convert them into stars.

In our models, photo-ionization due to a cosmic reionizing background and supernova feedback work together in order to re-shape this highly peaked luminosity function into the near-power law down to  $M_V \sim -3$  that is implied by the recent SDSS observations. Photo-ionization suppresses the infall of hot gas into low-mass dark matter haloes, reducing the supply of baryons that are available for cooling and star formation, while SN feedback reheats cold gas and expels it from small haloes, again suppressing the efficiency of star formation. If we include only photo-ionization or only SN feedback, we find an excess of intermediate luminosity satellites and a shortage of ultra-faint satellites (see also Kopeck et al. 2009). In agreement with previous works (e.g. Kravtsov et al. 2004), we find that the satellite luminosity function in our “standard” models depends only weakly on the assumed redshift of reionization.

We made use of results from the numerical hydrodynamic simulations of Gnedin (2000) to motivate our treatment of the suppression of gas infall due to the presence of a photo-ionizing background. A key parameter in this recipe is the “filtering mass”, or the halo mass below which the gas content is significantly reduced relative to the cosmic average. However, recent work by other groups (Okamoto et al. 2008; Hoft et al. 2006) has found that the filtering mass may be considerably smaller than the results of Gnedin (2000) suggested. We investigate the implications of modi-



fying the normalization and/or redshift dependence of the filtering mass as suggested by these works, and find that when a lower normalization of the filtering mass is adopted, the results are more sensitive to the redshift of reionization. We find that we can still reproduce the observed luminosity function with the lower filtering mass if we adopt a higher reionization redshift ( $z_r \sim 11$  instead of  $z_r \sim 7.5$ ).

We investigate the impact of stellar stripping on the observed luminosity function using the MORGANA model. We find that stellar stripping can only decrease the satellite stellar masses by at most about  $\approx 20\%$ , and therefore probably has only a minor effect on the satellite LF. However, we find that the modelling of tidal *destruction* of satellites does have a significant effect on faint end of the predicted LF.

We also compare our SAM predictions with the observationally derived MW satellite stellar mass function, and find good agreement. In addition, we can compare the SMF predicted by numerical simulations of the same dark matter haloes that we used to extract our merger trees, but including a numerical treatment of hydrodynamics, cooling, star formation, supernova feedback, etc. We find a rather remarkable agreement between the predictions of the SAMs and the numerical hydro results over the rather limited mass range that is available due to the limited numerical resolution of the hydro runs.

In this work, we have concentrated on the comparison with observations of two quantities, statistical distributions of satellite luminosity and stellar mass, although naturally the SAMs provide predictions of many other galaxy properties. This has been done mainly for two reasons: first because robust state of the art observational data have recently been made available for those two quantities and second because our goal was to directly address the so called missing satellite problem and the origin of the newly discovered ultra-faint population. We defer a more extensive explorations of other satellite properties (such as metallicity, gas content, star formation history, etc.) to a future work.

The semi-analytic models that we use in this work were originally normalized to reproduce global quantities such as the field galaxy luminosity function or gas fractions for relatively luminous galaxies ( $M_V \lesssim -16$ ). They have not previously been extensively tested against observations of galaxies on these very small mass scales. In the case of the K08 and S08 models, we found that the *identical* model ingredients and even parameter values used in the standard versions of these SAMs (e.g. Somerville et al. 2008, Kang et al. 2005) were also able to reproduce the MW satellite LF. In the case of the MORGANA model, we found that the SN feedback recipe in the original model (Monaco et al. 2007) had to be modified in order to reproduce the faint satellite population. In either case, we have gained important insights about the physical recipes incorporated in these models and their applicability over a wide range of galaxy mass scales.

Our study confirms and expands on previous works that address the so-called missing satellite problem using semi-analytic models and simulations. The main new contribution of our paper is the implementation of SAMs within merger trees extracted from numerical simulations with very high mass resolution (particle mass  $m_p \sim 4 \times 10^5 h^{-1} M_\odot$ ), in which each of our four Galaxy-sized halo simulations contains 2–4 million particles. Thus, unlike previous stud-

ies (e.g. Benson et al. 2002; Somerville 2002; Kravtsov et al. 2004) which compared only with the “classical” satellite population  $M_V = -9$ , we can resolve the very small subhaloes that may host the newly detected population of ultra-faint satellites. We also have the advantage of multiple simulations, unlike studies based on the Via Lactea simulation (Diemand et al. 2007) alone. Although our results are in qualitative agreement with studies based on simpler analytic recipes for assigning baryons to dark matter (sub)-haloes (e.g. Koposov et al. 2009), we showed that in our models, the MW satellite LF is shaped by a complex combination of different physical processes including tidal destruction, photo-ionization, and supernova feedback.

Our models neglect several other physical processes that have been discussed in the literature, and which may be important in shaping the properties of galaxies on these mass scales. Although we model the suppression of gas infall by a uniform cosmic radiation field after reionization, we do not account for the modification of the atomic cooling function by the radiation field, the possible photo-evaporation of gas from small haloes after reionization (Barkana & Loeb 1999), or photo-ionization by the nearby large galaxy (i.e., the radiation field of the Milky Way; e.g. Weinmann et al. 2007). Perhaps most importantly, we neglect cooling via molecular hydrogen, and the associated complex and poorly understood possible positive and negative feedback effects connected with the formation and destruction of  $H_2$  (see Ricotti, Gnedin & Shull 2008 for a recent summary of these issues). The fact that our models are nevertheless able to reproduce the bulk of the ultra-faint satellite population *may* indicate that these other processes operate at second order or cancel each other out, or may be simply a fortuitous coincidence. Certainly this bears further study.

A further concern is that standard SAMs are known to fail to reproduce the more detailed properties of satellites in larger mass hosts: although they correctly reproduce the *number* of satellites as a function of halo mass, several different SAM codes (including the ones considered here) have been shown to produce too large a *fraction* of red and passive satellites (e.g. Kimm et al. 2008 and references therein) compared with observations. The main cause of this difficulty is believed to be the standard assumption that the hot gas halo is immediately stripped when a satellite enters a larger host, thereby depriving satellites of any new supply of gas (see Kang et al. 2008 for a detailed discussion and possible solution). It is unclear whether this will impact our predictions for the very low-mass MW satellites — we defer this question to a future investigation.

If we accept this “baryonic” solution of the “missing satellite problem”, other interesting implications follow. Our analysis predicts that roughly 1/5 of the total number of subhaloes with a present-day bound mass  $M > 2 \times 10^7 M_\odot$  should be dark. In order to properly test this picture, a signature of the presence of these dark satellites is needed. One possibility is that they could be detected via gravitational lensing (e.g. Metcalf & Zhao 2002) since those small subhaloes will act as perturbers of the lensing signal coming from the main halo. Unfortunately recent results based on numerical simulations have shown that perturbations in the lensing potential induced by (dark) satellites are very small and unlikely to explain the anomalous flux ratios of some multiple lensed QSOs (Macciò et al. 2006; Macciò &

Miranda 2006). Another possibility would be detection of  $\gamma$ -rays from dark matter annihilation, as the presence of substructure boosts the  $\gamma$ -ray signal by a factor of 4 to 15 relative to smooth galactic models (Diemand et al. 2008). Finally, a third possible opportunity to detect the presence of a significant dark population of subhaloes in the MW halo could come from the signatures of the interaction of such a population with the thin stellar streams which are known to fill a large portion of the MW halo (Odenkirchen et al. 2001, Grillmair & Dionatos 2006).

In final summary, our results show that not only is there no longer a “missing satellite problem”, but that well-known and well-motivated astrophysical processes working within the  $\Lambda$ CDM framework *naturally* predict the form of the observed MW satellite luminosity function over six orders of magnitude in luminosity. Indeed, it may be that convincing proof of the existence of the large predicted population of dark subhaloes via one of the methods suggested above (or one not yet discovered) is one of the last remaining major challenges for the  $\Lambda$ CDM paradigm.

## ACKNOWLEDGEMENTS

The authors are grateful to Jelte de Jong, Anna Gallazzi, Nicholas Martin, Christian Maulbetsch, Hans-Walter Rix and Frank van den Bosch for many stimulating discussions. We thank Eric Bell for communicating unpublished results. Numerical simulations were performed on the PIA and on PanStarrs2 clusters of the Max-Planck-Institut für Astronomie at the Rechenzentrum in Garching and on the zBox2 supercomputer at the University of Zürich. Special thanks to B. Moore, D. Potter and J. Stadel for bringing zBox2 to life. FF and SK acknowledge the Kavli Institute for Theoretical Physics in Santa Barbara for hospitality: this research was partially supported by the National Science Foundation under Grant No. NSF PHY05-51164. SK was supported by the DFG through SFB 439 and by a EARA-EST Marie Curie Visiting fellowship.

## REFERENCES

- Adelman-McCarthy, J. K., et al. 2008, *ApJS*, 175, 297  
 Babul, A., & Rees, M. J. 1992, *MNRAS*, 255, 346  
 Barkana, R., Loeb, A., 1999, *ApJ*, 523, 54  
 Baugh, C. M. 2006, *Reports on Progress in Physics*, 69, 3101  
 Belokurov, V., et al. 2007, *ApJ*, 654, 897  
 Benson, A. J., Frenk, C. S., Lacey, C. G., Baugh, C. M., & Cole, S. 2002, *MNRAS*, 333, 177  
 Bertschinger, E. 2001, *ApJS*, 137, 1  
 Boylan-Kolchin, M., Ma, C.-P., & Quataert, E. 2008, *MNRAS*, 383, 93  
 Bruzual, G., & Charlot, S. 2003, *MNRAS*, 344, 1000  
 Bullock J. S., Kravtsov A. V., Weinberg D. H., 2000, *ApJ*, 539, 517  
 Chabrier G., 2003, *PASP*, 115, 763  
 Charlot, S., & Fall, S. M. 2000, *ApJ*, 539, 718  
 Cole, S., Lacey, C. G., Baugh, C. M., & Frenk, C. S. 2000, *MNRAS*, 319, 168  
 Diemand, J., Kuhlen, M., & Madau, P. 2007, *ApJ*, 667, 859  
 Diemand, J., Kuhlen, M., Madau, P., Zemp, M., Moore, B., Potter, D., & Stadel, J. 2008, *Nature*, 454, 735  
 Efstathiou, G. 1992, *MNRAS*, 256, 43P  
 Fontanot, F., Somerville, R. S., Silva, L., Monaco, P., & Skibba, R. 2009, *MNRAS*, 392, 553  
 Gilmore, G., Wilkinson, M. I., Wyse, R. F. G., Kleyna, J. T., Koch, A., Evans, N. W., & Grebel, E. K. 2007, *ApJ*, 663, 948  
 Giocoli, C., Tormen, G., & van den Bosch, F. C. 2008, *MNRAS*, 386, 2135  
 Governato, F., et al. 2004, *ApJ*, 607, 688  
 Governato, F., Willman, B., Mayer, L., Brooks, A., Stinson, G., Valenzuela, O., Wadsley, J., & Quinn, T. 2007, *MNRAS*, 374, 1479  
 Grillmair, C. J., & Dionatos, O. 2006, *ApJL*, 643, L17  
 Haardt, F., & Madau, P. 1996, *ApJ*, 461, 20  
 Hoefl, M., Yepes, G., Gottlöber, S., & Springel, V. 2006, *MNRAS*, 371, 401  
 Irwin, M. J., et al. 2007, *ApJL*, 656, L13  
 Jiang, C. Y., Jing, Y. P., Faltenbacher, A., Lin, W. P., & Li, C. 2008, *ApJ*, 675, 1095  
 Kang, X., Jing, Y. P., Mo, H. J., Börner, G. 2005, *ApJ*, 631, 21  
 Kang, X. 2008, *Proceedings of IAU 254 "The Galaxy Disk in Cosmological Context"*, arXiv:0806.3279  
 Katz, N. 1992, *ApJ*, 391, 502  
 Kimm, T., et al. 2008, *MNRAS* in press, arXiv:0810.2794  
 Klypin, A., Kravtsov, A. V., Valenzuela, O., & Prada, F. 1999, *ApJ*, 522, 82  
 Klypin, A., Zhao, H., & Somerville, R. S. 2002, *ApJ*, 573, 597  
 Knebe, A., Arnold, B., Power, C., & Gibson, B. K. 2008, *MNRAS*, 386, 1029  
 Komatsu, E., et al. 2009, *ApJS*, 180, 330  
 Koposov, S., et al. 2008, *ApJ*, 686, 279 (SK08)  
 Koposov, S. E., Yoo, J., Rix, H.-W., Weinberg, D. H., Macciò, A. V., & Miralda-Escudé, J. 2009, *ApJ* in press, arXiv:0901.2116  
 Kravtsov, A. V., Gnedin, O. Y., & Klypin, A. A. 2004, *ApJ*, 609, 482  
 Li, Y., Mo, H. J., van den Bosch, F. C., & Lin, W. P. 2007, *MNRAS*, 379, 689  
 Macciò, A. V., Moore, B., Stadel, J., & Diemand, J. 2006, *MNRAS*, 366, 1529  
 Macciò, A. V., & Miranda, M. 2006, *MNRAS*, 368, 599  
 Macciò, A. V., Dutton, A. A., van den Bosch, F. C., Moore, B., Potter, D., & Stadel, J. 2007, *MNRAS*, 378, 55  
 Macciò, A. V., Dutton, A. A., & van den Bosch, F. C. 2008, *MNRAS*, 391, 1940  
 Macciò, A. V., Kang, X., & Moore, B. 2009, *ApJL*, 692, L109  
 Madau, P., Kuhlen, M., Diemand, J., Moore, B., Zemp, M., Potter, D., & Stadel, J. 2008, *ApJL*, 689, L41  
 Mainini, R., Macciò, A. V., Bonometto, S. A., & Klypin, A. 2003, *ApJ*, 599, 24  
 Martin, N. F., Ibata, R. A., Chapman, S. C., Irwin, M., & Lewis, G. F. 2007, *MNRAS*, 380, 281  
 Martin, N. F., de Jong, J. T. A., & Rix, H.-W. 2008, *ApJ*, 684, 1075 (MdJR08)  
 Mateo, M. L. 1998, *ARA&A*, 36, 435  
 McConnachie, A. W., et al. 2008, *ApJ*, 688, 1009  
 Metcalf, R. B., & Zhao, H. 2002, *ApJL*, 567, L5

- Metz, M., Kroupa, P., & Jerjen, H. 2007, MNRAS, 374, 1125
- Monaco, P., Theuns, T., & Taffoni, G. 2002, MNRAS, 331, 587
- Monaco, P. 2004, MNRAS, 352, 181
- Monaco, P., Fontanot, F., & Taffoni, G. 2007, MNRAS, 375, 1189
- Moore, B., Ghigna, S., Governato, F., Lake, G., Quinn, T., Stadel, J., & Tozzi, P. 1999, ApJL, 524, L19
- Navarro, J. F., Frenk, C. S., & White, S. D. M. 1997, ApJ, 490, 493
- Odenkirchen, M., et al. 2001, ApJL, 548, L165
- Okamoto, T., Gao, L., & Theuns, T. 2008, MNRAS, 390, 920
- Parkinson, H., Cole, S., & Helly, J. 2008, MNRAS, 383, 557
- Peñarrubia, J., McConnachie, A. W., & Navarro, J. F. 2008, ApJ, 672, 904
- Quinn, T., Katz, N., & Efstathiou, G. 1996, MNRAS, 278, L49
- Read, J. I., Pontzen, A. P., & Viel, M. 2006, MNRAS, 371, 885
- Ricotti M., Gnedin N. Y., Shull J. M., 2002, ApJ, 575, 49
- Ricotti M., Gnedin N. Y., Shull J. M., 2008, ApJ, 685, 21
- Silva, L., Granato, G. L., Bressan, A., & Danese, L. 1998, ApJ, 509, 103
- Simon, J. D., & Geha, M. 2007, ApJ, 670, 313
- Somerville, R. S., Kolatt, T. S., MNRAS, 1999, 305, 1
- Somerville, R. S., Primack, J. R., MNRAS, 1999, 310, 1087
- Somerville, R. S., Primack, J. R., & Faber, S. M. 2001, MNRAS, 320, 504
- Somerville, R. S. 2002, ApJL, 572, L23
- Somerville, R. S., Hopkins, P. F., Cox, T. J., Robertson, B. E., & Hernquist, L. 2008, MNRAS, 391, 481
- Stadel, J. G. 2001, Ph.D. Thesis, University of Washington
- Stinson, G., Seth, A., Katz, N., Wadsley, J., Governato, F., & Quinn, T. 2006, MNRAS, 373, 1074
- Strigari, L. E., Bullock, J. S., Kaplinghat, M., Diemand, J., Kuhlen, M., & Madau, P. 2007, ApJ, 669, 676
- Strigari, L. E., Bullock, J. S., Kaplinghat, M., Simon, J. D., Geha, M., Willman, B., & Walker, M. G. 2008, Nature, 454, 1096
- Taylor, J. E., & Babul, A., 2004, MNRAS, 348, 811
- Taffoni, G., Mayer, L., Colpi, M., & Governato, F. 2003, MNRAS, 341, 434
- Thoul, A. A., & Weinberg, D. H. 1996, ApJ, 465, 608
- Tollerud, E. J., Bullock, J. S., Strigari, L. E., & Willman, B. 2008, ApJ, 688, 277
- Viola, M., Monaco, P., Borgani, S., Murante, G., & Tornatore, L. 2008, MNRAS, 383, 777
- Wadsley, J. W., Stadel, J., & Quinn, T. 2004, New Astronomy, 9, 137
- Walsh, S. M., Willman, B., & Jerjen, H. 2009, AJ, 137, 450
- Wechsler, R. H., Bullock, J. S., Primack, J. R., Kravtsov, A. V., & Dekel, A. 2002, ApJ, 568, 52
- Weinmann, S. M., Macciò, A. V., Iliev, I. T., Mellema, G., & Moore, B. 2007, MNRAS, 381, 367
- White, S. D. M., & Frenk, C. S. 1991, ApJ, 379, 52
- Willman, B., et al. 2005, ApJL, 626, L85
- Zentner, A. R., Bullock, J. S. 2003, ApJ, 598, 49
- Zentner, A. R., Berlind, A. A., Bullock, J. S., Kravtsov, A. V., Wechsler, R. H., 2005, ApJ, 624, 505
- Zucker, D. B., et al. 2006a, ApJL, 643, L103